NASA CONTRACTOR REPORT

NASA CR-1638

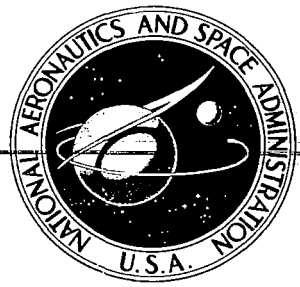

EXPERIMENTAL AND ANALYTICAL INVESTIGATIONS ON MULTIPLE LIQUID IMPACT EROSION

by A. Thiruvengadam, S. L. Rudy, and M. Gunasekaran

Prepared by
HYDRONAUTICS, INC.
Laurel, Md. 20810
for

NATIONAL AERONAUTICS AND SPACE ADMINISTRATION • WASHINGTON, D. C. • SEPTEMBER 1970

1. Report No.	2. Government Accession No.	3. Recipient's Catalog No.
NASA CR-1638		

4. Title and Subtitle: EXPERIMENTAL AND ANALYTICAL INVESTIGATIONS ON MULTIPLE LIQUID IMPACT EROSION

5. Report Date: September 1970

6. Performing Organization Code:

7. Author(s): A. Thiruvengadam, S. L. Rudy and M. Gunasekaran

8. Performing Organization Report No.: 719-2

9. Performing Organization Name and Address:
HYDRONAUTICS, Inc.
Pindell School Road
Laurel, Maryland 20810

10. Work Unit No.:

11. Contract or Grant No.: NASW-1608

12. Sponsoring Agency Name and Address:
National Aeronautics & Space Administration
Washington, D. C. 20546

13. Type of Report and Period Covered: Contractor Report

14. Sponsoring Agency Code:

15. Supplementary Notes:

16. Abstract

Research on the impact erosion of 1100-0 Aluminum, 316 stainless steel, commercially pure annealed nickel and annealed 6AL - 4V titanium is reported. The erosion is caused by multiple impacts with a water jet in a rotating disk facility. Relationships between the velocity of impact and the number of impacts at which visible indentations were observed are compared with the high frequency fatigue strength of these materials. Experimentally observed rates of erosion are compared with a recently developed theory of erosion, and with the fatigue life measurements. The peak rate of erosion varies approximately as the fifth power of the velocity of impact. The time to reach the peak rate varies as the one-fifth power of the velocity. Cavitation erosion strengths and liquid impact erosion strengths are also compared.

17. Key Words (Selected by Author(s))	18. Distribution Statement
Multiple liquid impact, erosion threshold, erosion rate, theory of erosion, high frequency fatigue, cavitation erosion, Weibull distribution	Unclassified - Unlimited

19. Security Classif. (of this report)	20. Security Classif. (of this page)	21. No. of Pages	22. Price*
U	U	84	$3.00

*For sale by the Clearinghouse for Federal Scientific and Technical Information
Springfield, Virginia 22151

ACKNOWLEDGMENT

The investigations reported herein were supported by the National Aeronautics and Space Administration under Contract NASW-1608. The authors are especially grateful to Mr. S.V. Manson of NASA headquarters for the personal interest in these studies and for his many useful discussions and suggestions.

TABLE OF CONTENTS

LIST OF FIGURES

SUMMARY

This report summarizes the results of experimental and analytical investigations on multiple liquid (water) impact erosion of four materials, namely 1100-0 aluminum, 316 stainless steel, commercially pure annealed nickel and 6AL-4V titanium alloy (annealed). Preliminary data are also reported for three turbine materials, namely Stellite 6B, Udimet 700 and a molybdenum alloy TZM. The erosion was produced in a rotating disk facility. Test specimens rotating in a horizontal plane cut vertical jets twice in one revolution. Using this facility, the relationship between the velocity of impact and number of impacts after which visible indentations were observed was established. For the same four materials, the fatigue strengths were also experimentally determined as a function of the number of cycles to failure in the high frequency fatigue apparatus. These two groups of data have been correlated in terms of the water hammer pressure.

Futhermore, the rate of erosion was determined as a function of the test duration for these test materials at different velocities. These data are compared with a recently developed theory of erosion. The fatigue life distribution curves are also included for these materials.

The peak rate of erosion varies as U^m where U is the impact velocity and m is an exponent. The present experiments indicate that m is close to 5, thus lending further support to some of the previous observations made by other investigators.

In order to compare cavitation erosion and multiple liquid impact erosion, cavitation erosion tests were conducted on the same four materials at a double amplitude of 3×10^{-3} inch and at a frequency of 13.5 kcs. The erosion strengths have been calculated for both types of erosion processes. While these two sets of erosion strengths rank the four materials in the same order, the actual values differ considerably.

INTRODUCTION

The problem of erosion caused by multiple liquid impacts can become a serious one in the development of future space nuclear power systems. In addition it is also important in wet steam or vapor turbines and in rain erosion of aircraft and missiles. The objectives of the present research program are the understanding of the mechanism and the quantitative evaluation of two aspects of multiple liquid impact erosion, namely; (i) the initiation of erosion and (ii) the rate of erosion. During the past several years of intensive research in the allied problem of cavitation erosion, the above two aspects were considered in depth (References 2 and 3). Some of the significant ideas generated through those efforts were extended to the understanding of multiple liquid impact erosion.

Specifically our attention was focused on the following aspects:

1. Determination of the relationship between velocity of impact and the number of impacts to produce visible erosion.

2. Determination of the relationship between the high frequency fatigue stresses and the number of cycles to failure.

3. Relating the water hammer stresses corresponding to the impact velocities with the high frequency endurance limit.

4. Determination of the rate of erosion as a function of exposure time.

5. Correlation of the experimental rates with a recently developed theory.

6. Evaluation of the dependence of the rate of erosion on the velocity of impact.

7. Comparison of liquid impact erosion strength and cavitation erosion strength for these four materials.

These investigations were initiated during April 1967. A technical report containing the results for 1100-0 aluminum and 316 stainless steel was issued at the end of the first year of this program (Reference 1). Additional tests on commercially pure nickel and titanium (6AL-4V) were conducted during the second year starting May 1968. This report contains a complete analysis of all of these results including the results of 1100-0 aluminum and 316 stainless steel in order to give an overall review of the accomplishments. A comparison of cavitation erosion

and multiple liquid impact erosion is made for the four test materials in terms of their erosion strength. Preliminary data on impact erosion of three turbine materials (Stellite 6B, Udimet 700 and a molybdenum TZM are also included.

EXPERIMENTAL FACILITY AND TECHNIQUES

The Jet Impact Erosion Facility

The jet impact erosion facility (Figure 1) consists of a rotating disk driven by a 2-1/2 hp variable speed motor capable of sustained operation at 20,000 rpm. The rotating disk is capable of holding six specimens as shown in Figure 1. The disk rotates in the horizontal plane cutting two sets of 1/32 inch diameter vertical jets as shown in Figures 2 and 2a. The dimensions of the rotating disk are shown in Figure 3. The erosion was caused by the impact of the test specimens on the solid jet at controlled speeds. Further details on the design, fabrication and operation of this facility are available in Reference 1. This test apparatus is similar to the one reported by Ripken (5) in many respects.

High Frequency Fatigue Testing Technique

A magnetostriction oscillator (Figure 4) was used to produce alternating strains at the node of a resonating rod. The basic

principle and the practical aspects of these tests are described in Reference 4. The fatigue specimen design used in the earlier studies had a sharp notch at the node. The notch sensitivity of the test materials at high frequencies is an unknown. In order to eliminate this limitation, a new dumb-bell shaped fatigue specimen was designed and used for all the fatigue tests under this program.

The basic approach for the design of the fatigue specimen is to use the theory developed by Neppiras (6). From this theory one can get the lengths of the fatigue specimen as shown by the example in Figure 5. Assuming an area ratio and ℓ_1/λ the value of ℓ_2/λ may be determined from Neppiras' theory. In order to avoid the sharp corners, a circular arc fillet of radius R is used. The value of R can be calculated from simple geometrical considerations. This method of designing dumb-bell shaped fatigue specimens gave the dimensions within 10 to 15 percent accuracy. Then the final adjustments are made by tuning experimentally. The dimensions of a properly tuned fatigue specimen are shown in Figure 6.

In all the fatigue studies, theoretical strain, given by the following formula (due to Neppiras (6)), was assumed to be the actual value:

$$\epsilon = \frac{G.2\pi\xi}{\lambda} \qquad [1]$$

where

ϵ - the strain amplitude at the node,

ξ - the displacement amplitude at the anti-node,

λ - the wavelength in the material, and

G - Magnification Factor

$$= \frac{\text{Strain in stepped specimen}}{\text{Strain in uniform specimen (without step).}}$$

The value of G can be calculated from Neppiras' theory. Generally one would measure the displacement amplitude ξ and the wavelength λ, and calculate the strain using a theoretical value of G. However, we verified these calculations by measuring the actual strains generated at the node (Figure 7).

EXPERIMENTAL PROCEDURE

As discussed previously, essentially the following three types of experiments were performed during this investigation:

1. Determination of threshold velocities,
2. Determination of the fatigue endurance limit, and
3. Determination of erosion rates both by multiple liquid impacts and by cavitation.

The impact erosion tests were carried out in the jet impact erosion facility; the fatigue tests and cavitation erosion tests were conducted in the magnetostriction vibratory apparatus. The important details of the experimental procedure followed are described below.

Determination of Threshold Velocities

Six test specimens were attached at three radial locations in the rotating disk described previously. This enabled the observation of two specimens at a preselected test velocity ensuring the reproducibility and reliability of the experimental observation. The test specimens were 3/8 inch in diameter. The specimen surface was finished to 32 rms or better by hand polishing, thus eliminating the possibility of mechanical work hardening affecting the test results. Such carefully prepared test specimens were attached to the rotating disk and run at preselected speeds. Observation of the specimens to determine when denting or fracture occurred was adjusted to suit the test sequence. When tests were conducted at higher velocities, damage could be observed in a short time and hence the specimens were observed at short intervals (every few minutes). At lower velocities, damage would not occur for many hours, consequently observations were made every half or one hour. The observation consisted of removing a test specimen and of observing the surface exposed to liquid impact with a 10 X magnifying glass under side lighting which would make the initial indentations "stand out" when illuminated at the proper angle to the surface. The time taken for the initiation of permanent plastic indentations on the surface of the test specimen through this procedure was recorded at different test velocities. The number of impacts were calculated from the number of revolutions made during that time multiplied by

two for the two impacts per revolution. The relationship between the number of impacts to initiate erosion and the corresponding threshold velocity was plotted.

After the appearance of plastic dents on the specimen surface, this area of denting will continue to work harden as the test progresses, resulting in the fracture of small fragments of material from the surface. In all our experiments, the criterion for threshold was the appearance of detectable indentation with the help of a 10 X magnifier under side lighting. The appearance of the surface after 10 million impacts at 150 fps on 316 stainless steel is shown in Figure 8. Surface roughness profiles after 10 million impacts at threshold of erosion and at fracture are shown in Figure 9.

Determination of High Frequency Endurance Limit

The fatigue specimens were vibrated at 14.2 kcs at controlled amplitudes in the magnetostriction vibratory apparatus. The specimens were cooled by immersion in a constant temperature water bath. The amplitude was obtained from the voltage output of a precalibrated voice coil. The strain was calculated from the amplitude (using Equation 1) as discussed previously. The stress was obtained by multiplying the strain with the modulus of elasticity. The modulus of elasticity for the test material can also be determined with the vibrator by measuring the wavelength and the frequency which will give the speed of sound.

The frequency was accurately measured with a frequency counter. The time to failure was noted and the number of cycles to failure was computed from the frequency.

Determination of Rate of Erosion as a Function of Exposure Time

The rate of weight loss was determined periodically by weighing the same specimen after exposure to impact at pre-selected velocities or to cavitation at 3×10^{-3} inch double amplitude. Care was taken to adopt a uniform procedure in cleaning and drying the specimen before and after each test. The erosion rate at time t was computed by dividing the incremental weight loss, ΔW, by the incremental time, Δt, during the time period $t-\Delta t$ to t. The mean depth of erosion was calculated by dividing the volume of erosion by the area of erosion. The eroded area was taken to be equal to the impact area of the jet. The actual eroded area can also be measured accurately with a planimeter.

RESULTS AND ANALYSIS

Correlation of Water Hammer Stresses with High Frequency Endurance Limits

Figure 10 shows the relationship between the velocity of impact and the number of impacts after which indentations were observed on all four test materials.

When a cylindrical column of liquid impinges on the surface of a material, the maximum stress developed at the point of contact by the impact (generally known as "water hammer" stress) is derived by de Haller (7) as

$$\sigma_I = \frac{\rho_\ell C_\ell U_I}{1 + \frac{\rho_\ell C_\ell}{\rho_m C_m}} \qquad [2]$$

where

U_I = impact velocity,

ρ_ℓ = density of liquid,

ρ_m = density of material,

C_ℓ = velocity of sound in liquid, and

C_m = velocity of sound in the material.

For the present investigations in which water was the test liquid and common metals are the test materials, the ratio $\rho_\ell C_\ell / \rho_m C_m$ is small compared to unity. Then the water hammer stress becomes

$$\sigma_I = \rho_\ell C_\ell U_I \qquad [3]$$

The values of $\rho_\ell C_\ell U_I$ were calculated for the data shown in Figure 10. The values of ρ_ℓ and C_ℓ for water were obtained from published literature (for example Reference 8).

The ratio of the high frequency fatigue strength to the water hammer stress for erosion inception is shown in Figure 11 for each of the four materials tested. Figure 11 shows that for all the materials tested, the ratio appears to be independent of the number of cycles to failure. This lends support to the concept previously proposed by Thiruvengadam (2) that impact erosion is the result of failure in fatigue.

The correlation in Figure 11 shows that for commercially pure annealed nickel, plastic indentations occur on the surface at an impact water hammer stress that is one third of the fatigue stress necessary to fracture the material. The data for titanimum shows that the water hammer stress to erosion inception is only one fifth of the stress required to fail the material in fatigue. Thus the ratio $\sigma_\alpha / \rho_\ell C_\ell U_I$ for erosion inception varies among materials.

We tentatively suggest that this may be explained in terms of notch sensitivity. The titanium alloys are in general very sensitive to stress concentrations (9). The fatigue data shown in Figure 11 are obtained with dumb-bell shaped fatigue specimens

thus eliminating any notch effects. However, the impact stresses are produced locally. This may possibly lead to stress concentrations at the grain boundaries causing local fatigue failures. Thus the use of a notched specimen may be preferable to an unnotched specimen when comparing impact erosion and fatigue failure. Experimental exploration of this concept would be desirable.

Effect of Time of Exposure to Multiple Liquid Impacts on the Rate of Erosion

The importance of exposure time on the rate of erosion was recognized and highlighted in a series of recent publications (10,11,12,13 and 14) based mainly on cavitation erosion research. This relationship was divided into four periods*, Figure 12, as follows:

1. Incubation period: The rate of erosion is very small during the early part of an erosion test. During this time, the material undergoes permanent changes due to the repeated erosive forces. Hence it is believed that the erosion incubates during this period.

2. Acceleration period: After the incubation, the material starts fracturing due to the repeated impacts. The rate of loss of material starts increasing with further exposure to erosion. Since this process is similar to cumulative fatigue fracture, it may also be called energy accumulation period.

---

* These terms correspond to the recently developed definitions by the ASTM Sub-committee headed by Dr. Robert Hickling.

3. Deceleration period: Where enough material has been fractured, the eroded surface becomes rough with visible deep craters. In cavitation erosion and in liquid impact erosion, the liquid covering these craters cushions the impact pressures transmitted to the material. The decrease in erosion rate is believed to be due to this attenuation process and hence this period may also be called the attenuation period.

4. Steady period: It is experimentally observed that after the attenuation period, the rate of erosion becomes very nearly independent of the exposure time and hence it is called the steady period.

Although the above results on the effect of exposure time were observed only for cavitation erosion, there were some indications in the literature that these effects were also detectable in liquid impact erosion tests such as steam turbine erosion (15, 16), jet impact erosion (17) and rain erosion (18). A summary and discussion of all these results with a mathematical analysis was presented by Heymann (19).

At this juncture, it became crucial to conduct a few systematic experiments to accumulate quantitative data in the case of multiple liquid impact erosion. Such results are shown in Figures 13 through 16, for the four test materials. The results shown correspond to six velocities for each material. It may be noted that the incubation period is very noticeable at lower

speeds whereas the peak rate of erosion is very pronounced at higher impact speeds.

It is necessary to understand and predict these non-linear time effects quantitatively in order to achieve meaningful correlations in the laboratory and to extrapolate laboratory data to field systems. With this aim in mind, an elementary theory of erosion has been developed recently (3) and is summarized briefly in Reference 1.

Correlation with the Theory of Erosion

An elementary theory of erosion detailed in References 1 and 3 yields the following equation for the normalized erosion rate as a function of the normalized time:

$$\bar{I} = \frac{\bar{\eta}}{\left[1 + \bar{K}\,\frac{n+1}{n}\int_{1}^{\tau} \bar{\eta}\, d\tau\right]^{\frac{n}{n+1}}} \qquad [4]$$

where

$\bar{I} = \frac{r}{r_{max}}$ = relative intensity of erosion

r = the rate of erosion at any time, t

t = the time corresponding to erosion rate, r,

r_{max} = the maximum rate of erosion

t_1 = the time at which maximum erosion rate occurs.

$$\tau = \frac{t}{t_1}$$

η = the efficiency* of erosion at any time, t,

η_1 = the efficiency corresponding to the peak rate of erosion,

$\bar{\eta} = \eta/\eta_1$

$$\bar{K} = \left(\frac{d\bar{\eta}}{d\tau}\right)_{\tau=1} \quad \text{and}$$

n = the attenuation exponent

In order to calculate $\bar{I}$ as a function of τ, the value of n and the function $\eta(t)$ must be known. These are discussed as follows: From the experience of underwater explosions, it is known that the shock pressure attenuates inversely as the distance travelled (20). Since the intensity (power transmitted per unit area) varies as the square of the shock pressure, the attenuation exponent, n, is herein assumed to have the value 2. Thus, by assumption,

$$n = 2 \qquad [5]$$

* The efficiency of erosion represents the ratio of the energy absorbed by the material to the energy of impact on the surface.

In the original formulation of the elementary theory (3), the nature of the function $\eta(t)$ was assumed to be similar to the fatigue probability function. The physical basis for this assumption may be stated as follows: A fractured particle has absorbed energy from the impact forces over a number of cycles. After the cumulative absorption of these impact forces, the particle fractures from the specimen thereby producing a loss of material. In this sense, the efficiency of the erosion process is associated with the fracture of a particle of the material. If we consider the particle as a fatigue specimen, then the probability of failure of the particle after some time is a statistical function. Based on this approach, it may be inferred that the efficiency of energy absorption (the function $\eta(t)$) is associated with the probability of failure of a particle after a given time. There are several statistical distribution functions advanced in the literature to represent the probability of fatigue failure. Specifically, the Weibull distribution (21) was chosen for the initial analysis because of its wide applicability. Hence a Weibull type distribution function of the following form was assigned to η:

$$\eta = 1 - \exp(-\tau^{\alpha}) \qquad [6]$$

The parameter α is called the Weibull shape parameter and it depends upon the material as well as the stress level. Wide applicability of the Weibull distribution can be seen from the fact that the function given by Equation [6] becomes a simple exponential distribution when $\alpha = 1$ and the Rayleigh distribution

when $\alpha = 2$; it corresponds to a nearly normal distribution when $\alpha = 3.57$ (22). From Equation [6] it followed as shown in Reference 1, that

$$\eta_1 = \frac{e-1}{e}$$

$$\bar{\eta} = \frac{e}{e-1}\left[1 - \exp(-\tau^{\alpha})\right]$$

and

$$\overline{K} = \frac{\alpha}{e-1}$$

where

e = the base of natural logarithms
= 2.7183

Employing these values, Equation [6] takes the form

$$\overline{I} = \frac{r}{r_{max}} = \frac{\frac{e}{e-1}\left[1 - \exp(-\tau^{\alpha})\right]}{\left[1 + \frac{1.5\alpha}{e-1}\int_1^{\tau} \frac{e}{e-1}\left[1 - \exp(-\tau^{\alpha})d\tau\right]\right]^{\frac{2}{3}}} \qquad [7]$$

Equation [7] shows that when the assumptions indicated in Equations [5] and [6] are employed, the normalized erosion rate at any normalized time, τ, depends on a single constant, α. As

indicated above, the numerical value of α depends on the material being eroded and on the magnitude of the impact stress. Using a series of constant values of α in Equation [7], the normalized erosion rate r/r_{max} can be plotted as a function of relative exposure time τ with α as the parameter.

At this juncture, the following points about the elementary theory discussed above are worthy of consideration:

1. The theory is not limited to the use of Weibull type distributions to represent the efficiency of energy aborption. In fact, it is also possible to use a direct relationship between the energy absorption capacity and the number of impacts. As of now no such quantitative relationship exists although one may develop an empirical relationship to fit the available experimental data. For example Manson (23) has presented experimental evidence to show how work hardening or work softening of metals proceeds with number of fatigue cycles. The fact that the phenomenon of work hardening or work softening is important in the erosion process has been pointed out by many investigators including Engel (24). However, the state-of-the-art is not adequate to develop a general mathematical relationship to fit the experimental data. For this reason, the Weibull type distributions were used as a first attempt.

2. In the elementary theory only the efficiency function $\eta(t)$ was assumed to be a statistical distribution.

However, the drop size distribution (or bubble size distribution in the case of cavitation) and the surface roughness distribution are both statistical quantities. For this reason, it was pointed out in Reference 3 that a general theory of erosion would lead to an erosion distribution function, which would take into account all of the above parameters.

3. Again, it was assumed in the elementary theory, that the value of the shape parameter α, was exactly the same as one would obtain from a fatigue life distribution for the material. Another assumption involved is that the value of α is unique at all stress levels. However, it is known that the value of the shape parameter depends upon the stress level, the presence of notches, the environment and the material (21).

With this background, the experimental data shown in Figures 13 through 16 may be reduced to the non-dimensional form by dividing the rate of loss at any time by the peak rate of loss, the latter being obtained from the curve which fitted the experimental data best. The time is normalized with respect to the time at which the peak erosion rate is observed. Figures 17 through 20 show the relative intensity of erosion as a function of the relative exposure time for the four metals tested. The solid lines in these figures are theoretical predictions of Equation [7] obtained by employing a constant value of α for each material in Weibull distributions of the type given by

Equation [6]. The agreement between the experimental and predicted curves appears reasonable and lends support to the use of the Weibull distribution as a first approximation to the efficiency function $\eta(t)$. As pointed out earlier, the value of α is different for different materials and is determined from the experimental data by the best fit. Thus, α becomes another material parameter in addition to the erosion strength, S_e.

Weibull Shape Parameters in Fatigue and Erosion

How does the value of the shape parameter, α as determined in the above erosion tests compare with the shape parameter, α as obtained from an actual fatigue life distribution for each material? In order to make a distinction between the two shape parameters, let us call the shape parameter for the erosion distribution α_1, and the shape parameter for the fatigue life distribution α_2.

The fatigue life distribution for the four materials were experimentally determined using the high frequency fatigue technique described earlier in this report and shown in Figures 21 through 24. These data show that the fatigue life distribution consists of two parts as shown in Figures 21 through 24. This is very similar to the two distribution interpretations given by Swanson (25). According to Swanson, there are two distributions at lower stress amplitudes (and hence at high life cycles) with two shape parameters. This is generally confirmed by our test results shown in Figures 21, 22 and 24. In order to see what

happens at higher stress levels we tested commercially pure nickel at a stress level corresponding to mean life in the range of 10^6 - 10^7 cycles. As shown in Figure 24, the results tend to show a single distribution corresponding to an average value of shape parameter $\alpha_2 = 3$. Thus it becomes clear that the shape parameter α_2 depends upon the stress level. The erosion was produced at much higher stress-levels since the particles were fractured and removed from the surface of the test specimens within a few thousand impacts at the most. Moreover, the fracture in erosion is produced at sharp corners causing stress concentrations whereas the dumb-bell shaped fatigue specimen is rather idealized when compared to the fractured particle. Hence the data support the use of a single value of α as a first approximation in analysis of erosion. As pointed out by Heymann (19) and by Thiruvengadam (3), the influence of other contributing factors such as surface roughness distribution and drop distribution must also be considered in addition to the fatigue life distribution.

While these aspects are under continued investigations, the results so far obtained do provide very useful practical results. For example, the effect of test duration may be quantitatively reduced in a generalized form. It can be mathematically expressed if the shape parameter α is determined through an erosion test for each material. This relationship can be integrated so that the cumulative depth of erosion may be predicted at different intensities of erosion.

The Relationship Between the Impact Velocity and the Rate of Erosion

The relationship between the velocity of impact and the rate of erosion is very important in understanding the phenomenon of erosion as well as in extrapolating laboratory data to practical problems. Heymann (26) has summarized most of the available information on this aspect. Without considering the effect of test duration, several investigators have found that the rate of erosion varies as some power of the impact velocity as listed below (26):

Author	Exponent
Honegger	2.0
Pearson	2.6
Hoff et. al.	5 - 7
Hobbs	5

After analyzing all these data, Heymann (26) came to the conclusion that the exponent will generally be of the order of 5. The experimenters (whose data were used by Heymann for his empirical analysis and discussion) did not consider the interacting effect of test duration on the velocity effects. Only recently is the importance of test-duration being recognized by various experimenters.

In our analysis the peak rate of volume loss as shown in Figures 13 through 16 are plotted as a function of impact velocity in Figure 25. The solid lines in Figure 25 correspond to a fifth power variation. In other words, the peak rate of erosion varies nearly as the fifth power of the velocity of impact. Similarly the time at which the peak rate is observed is also shown plotted against impact velocity in Figure 26 and the solid lines in this figure correspond to a one fifth power variation. To summarize these results,

$$I_{peak} \propto U^{5} \text{ (approximately)} \qquad [8]$$

$$t_1 \propto U^{1/5} \text{ (approximately)} \qquad [9]$$

where

I_{peak} - is the maximum intensity of erosion,

t_1 - is the time at which the peak intensity is observed, and

U - is the impact velocity.

Several investigators including Heymann have advocated a relationship of the form

$$I_{peak} \propto (U-U_T)^{m}$$

where U_T is the threshold velocity. The introduction of threshold velocity is very useful mainly because this avoids the

implication in Equation [8] that some erosion will occur even at very low impact velocities. When we included the threshold velocity in our analysis, the exponent, m, was still close to 5 (1). This is somewhat inconsistent with Heymann's conclusion that the exponent is in between 2.3 and 2.7. Additional investigations are needed in order to resolve this aspect.

COMPARISON OF LIQUID IMPACT EROSION STRENGTH AND CAVITATION EROSION STRENGTH

During the 1965 ASTM Symposium on Erosion by Cavitation or Impingement, Thiruvengadam (2) suggested a definition of erosion strength and a method to determine the erosion strength from an erosion test. Using this approach, the erosion strengths for the four test materials studied under this program were determined both for multiple liquid impact erosion and for cavitation erosion produced in a vibratory apparatus. The procedure for the determination of the erosion strength is as follows:

The intensity of erosion, defined as the power absorbed by the material per unit area, is given by

$$I = \left(\frac{\Delta V}{A_e}\right) \frac{S_e}{t} = \frac{iS_e}{t} \qquad [10]$$

where

ΔV is the volume of erosion,

t is the exposure time,

A_e is the area of erosion

i is the average depth of erosion, and

S_e is the erosion strength

In a given erosion test, the rate of volume loss is time dependent. Hence it becomes essential to choose a characteristic rate of volume loss. In Reference 2, the steady state rate was taken as the characteristic rate of volume loss, thus eliminating the interacting time dependence. However it takes quite a bit of time before steady state is reached, especially for stronger materials. For this reason, we selected in the present report the peak rate of erosion as the characteristic value. The peak rate and the steady state rate are related as shown in Figures 17 through 20.

The peak rates of volume loss for the four materials are shown in Table 1. These values are obtained from Figure 25. The projected area of the cylindrical jet (1/32" x 3/8") is taken as the area of erosion. From these data, the peak rate of depth of erosion is computed for each material. Adopting commercially pure annealed nickel as the standard material whose strain energy is identically equal to its erosion strength, the intensity of erosion is computed. The value for the strain energy for nickel used is 20,000 psi as reported in the literature (for example Reference 27). At 350 fps, the peak intensity

is computed from Equation [10] to be about 18 watts per square meter. Using this value of the intensity, the erosion strengths for the other three metals are computed as shown in Table 1.

Similarly, cavitation erosion tests were conducted in the magnetostriction vibratory apparatus using distilled water as the test liquid. The results are shown in Figures 27 through 30. The peak rates of erosion are tabulated in Table 2. The intensity for this case is calculated from Equation [10] to be about 2.5 watts per square meter. The cavitation erosion strengths of the four test materials are also shown in Table 2. While the ranking of the metals are the same both for the multiple liquid impact erosion and for cavitation erosion, the actual numbers do not agree. Before any definite conclusion may be reached, more investigations along these lines are necessary.

IMPLICATIONS OF THESE RESULTS FOR POTASSIUM AND CESIUM VAPOR TURBINES

The ultimate objective of these studies is to use the results in the design of erosion free space power systems. Specifically the current interest lies in the liquid metal vapor turbines with potassium or cesium as working fluids (e.g., 28). In view of this, it becomes important to consider some of the implications of the present study for potassium and cesium turbines. The parameters of interest in practical turbines are:

1. the size and shape of drops
2. the number of impacts
3. the relative drop impact velocities
4. the angle of impact of the drops, and
5. the resistance of candidate materials.

Each of these parameters is discussed in this section in light of the results generated under the current program.

Shape and Size of Drops

Although the water jet used in the present studies looks solid before impact, the observation of eroded surfaces on aluminum shows spherical indentations resembling drop impact phenomena. The diameter of the jet used in the laboratory experiment is 1/32 inch. This corresponds to 795 microns (795 x 10^{-6} meters). This compares well with the observation of Christie and Hayward (29) who in 1965 reported their observations in an operating steam turbine using a periscope and a movie camera. The drops had a maximum diameter of 450 microns. Pouchot (30) of Westinghouse Astronuclear Laboratory estimated a maximum of 130 microns for the drops in the third stage of the NASA - GE potassium vapor turbine. The British group (Baker, Elliott, Jones and Pearson (31)) working at the Central Electricity Board, use a drop size spectrum with a mean drop size of 660 microns in their apparatus.

Number of Impacts

The information on the number of drop impacts at a given location on the turbine blade in a given period of observation is very scarce due to the obvious difficulties in obtaining such information. However, Gyarmathy (32) makes a computation for a typical steam turbine blade rotating at tip speed of 820 fps and comes up with an estimate of 13 impacts per second at a given location. This corresponds to 5×10^8 impacts in 10,000 hours.

Relative Drop Impact Velocities

The relative velocity of the drop normal to the blade depends very much on the blade angle, the relative speed of the drop and many other factors controlling the dynamics of the drops in the short distance. A preliminary analysis shows that drop impact velocities may be of the order of 40 to 50 percent of the tip speed depending upon the specific case. For the typical steam turbines the relative impact speeds would range from 500 fps to 1000 fps. There may be fewer drops of larger size impinging at velocities higher than this velocity range.

It is interesting to note that the relative impact velocities for the NASA - GE potassium vapor turbines were estimated by three groups of scientists independently and reported at the October 15, 1968 conference at Cincinnati as follows:

	Pitch	Tip
Westinghouse Electric Company	440 fps	530 fps
General Electric Company	280 fps	440 fps
HYDRONAUTICS, Incorporated	260 fps	400 fps

Angle of Impact of the Drops

Experiments by Fyall et al (33) and Hoff et al (34) have shown that the threshold velocity is independent of the angle of incidence of the drops if the normal component of the impact velocity is considered.

The Resistance of Candidate Materials

The following quotation from Baker et al (31) illustrates the state-of-the-art up to 1967.

"At blade tip velocities above about 300 meters per second, the erosion damage suffered by conventional blading materials, such as 12% chromium type steels, is unacceptable and the leading surfaces of blades are fitted with shields of a more erosion resistant material such as high speed tool steel or cobalt chromium base alloys. However, the blade tip velocities encountered in the 500 MW machines now being commissioned are in excess of 500 meters per second and there is a need for more resistant materials."

It is important to note that the actual drop impact velocities corresponding to a blade tip speed of 300 meters per

second may range from 500 fps and upwards. Moreover, the test data by Baker et al show that all the candidate materials they tested showed substantial erosion in less than 100 hours of testing at an impact velocity of 1000 fps. For example, the Stellite 6 lost about 100 mg/cm^2 in less than 30 hours test at a velocity of 1000 fps. Some of their newly developed cobalt chromium alloys lost about 100 mg/cm^2 in about 150 hours at this test velocity.

The extent of erosion problems in the steam turbines operating in U. S. A. are well documented by Sajben (35) with comparative photographs. A more recent discussion appears in a survey by Fraas, Young and Grindell (36).

In order to determine the erosion resistance of some of the candidate materials for the NASA space power systems, we tested the following three materials in our test facility:

1. Stellite 6B
2. Udimet 700,
3. TZM

The test liquid was laboratory tap water at $68^{\circ}F$. Figures 31, 32, and 33 show the relationship between impact velocity and the number of impacts at which the erosion was observed. In each figure two sets of observations are recorded. One is the number of impacts at which the inception of plastic denting was observed at 10 X magnification. The other is the number of impacts at which visible fracture was observed on the surface.

According to these experiments, the threshold velocities corresponding to a million water impacts at room temperature are 350 fps, 310 fps and 225 fps for Stellite 6B, TZM and Udimet 700 respectively. As shown in Table 3, the ρC values for liquid potassium and for liquid cesium are about 70 percent of that for water. If we assume that the mechanical properties do not deteriorate very much with temperature and that the corrosive interaction is not much, then the threshold velocities corresponding to a million liquid metal impacts would be of the order of 500 fps, 440 fps and 320 fps for Stellite 6B, TZM and Udimet 700 respectively. Although the assumptions concerning the temperature effects and the corrosion effects are not valid, the actual operating experience of the NASA - GE potassium vapor turbine supports these projections. Young and Johnston (37) conducted cavitation erosion tests in liquid sodium at $800^{\circ}F$ on Stellite 6B and Udimet 700 and found that Stellite exhibited better erosion resistance as compared to Udimet 700. This supports our finding although our result is based on the threshold of these materials (much before the actual fracture of the material occurred) whereas the experiments by Young and Johnston (37) considered the resistance of these materials when the material was actually fractured from the surface. For further clarification of this problem additional systematic experiments would be required.

Considering the fact that the present investigations are of basic nature and that they are in their early stages, the above results show that these investigations are highly relevant in understanding and solving the practical problem of turbine erosion in service.

CONCLUDING REMARKS

The systematic investigations presented in this report lead to several interesting results. For example, the threshold water hammer pressure is nearly 1/2 to 1/3 of the fatigue endurance limit for the corresponding stress cycles as seen in Figure 11. Why should visible erosion be initiated at a stress much lower than the failure stress level? The answer to this question is not very clear at present. There are several cursory explanations. The plastic indentations may be produced at a much lower stress level than the fatigue stress necessary to fracture the metal. The structural properties of the material may also be important as indicated by the titanium alloy. Near threshold, the effect of corrosive interaction may be equally important. The one-dimensional analysis leading to the de Haller equation (Equation 2) may not be adequate to predict the impact pressure produced by liquid impact. In spite of these unresolved questions the results presented in Figures 10 and 11 are very useful as a guide to the designer.

The rate of erosion caused by multiple liquid impact is very much dependent on the exposure time. An attempt has been made to correlate these experimental data with the erosion theory recently developed to predict cavitation erosion. The shape parameter obtained in a high frequency fatigue curve at stress levels corresponding to a life in the range of 10 million cycles is much lower than the shape parameter required to predict the erosion rates. However when the distribution curve is generated at a higher stress level corresponding to a life in the range of 10^6 - 10^7 cycles, the shape parameter obtained in the fatigue distribution is closer to the shape parameter for the erosion distribution.

The erosion strengths of these four materials have been evaluated both for the multiple liquid impact erosion and for cavitation erosion. While the ranking of the materials is the same for both types of erosion, the actual values of erosion strengths do not agree.

The peak rate of erosion varies as the fifth power of the velocity of impact. The time at which the peak rate of erosion is observed varies as the one-fifth power of the impact velocity. This result is particularly interesting because the interacting influence of testing time is also considered in this correlation in contrast to the previous attempts. Furthermore, the inclusion of threshold velocity in the correlation does not reduce the

value of the exponent substantially. Although the previous investigations do point out a reduction in the exponent, further investigations on this aspect are needed to elucidate this point.

REFERENCES

1. Thiruvengadam, A. and S. L. Rudy, "Experimental and Analytical Investigations on Multiple Liquid Impact Erosion," HYDRONAUTICS, Incorporated Technical Report 719-1 dated June 1968. Also as NASA Contractor Report NASA CR-1288, Washington, D. C. March 1969.

2. Thiruvengadam, A., "The Concept of Erosion Strength," HYDRONAUTICS, Incorporated Technical Report 233-9, December 1965. (See Proc. Symp. on Erosion by Cavitation or Impingement, ASTM Annual Meeting 1966, ASTM Special Publication No. 408, Philadelphia, 1967).

3. Thiruvengadam, A., "Theory of Erosion," HYDRONAUTICS, Incorporated Technical Report 233-11, March 1967. (See also Proc. Second Meersburg Conference on Rain Erosion, August 1967. Published by Royal Aircraft Establishment, Farnborough, England).

4. Thiruvengadam, A., "High Frequency Fatigue of Metals and Their Cavitation Damage Resistance," Technical Report 233-6 HYDRONAUTICS, Incorporated, December 1964. (See also Paper 65-WA-UnT-4, Journal of Engineering for Industry, Transactions, AM. Soc. Mechanical Engrs. Vol. 88, Series B, No. 3, August 1966).

5. Ripken, J. F., "A Test Rig for Studying Impingement and Cavitation Damage," Erosion by Cavitation or Impingement, ASTM Special Technical Publication No. 408, American Society for Testing Materials, 1967.

6. Neppiras, E. A., "Techniques and Equipment for Fatigue Testing at Very High Frequencies," Proc. ASTM, Vol. 59, 1959, pp. 691-709.

7. Bowden, F. P., and Brunton, J. H., "The Deformation of Solids by Liquid Impact at Supersonic Speeds," Proc. Royal Society, London, A., Vol. 263, October 1961, pp. 433-450.

8. Greenspan, M. and Tschiegg, C. E., "Speed of Sound in Water by a Direct Method," Jour. Research of the National Bureau of Standards, Vol. 59, No. 4, October 1957.

9. Mann, J. Y., "Fatigue Problems Associated with Structural Materials for Current and Future Aircraft," Structures and Materials Report 270, Australian Defence Scientific Service Aeronautical Research Laboratories, September 1959.

10. Thiruvengadam, A., "A Comparative Evaluation of Cavitation Damage Test Devices," HYDRONAUTICS, Incorporated Technical Report 233-2, November 1963 (See also Proc. Symp. on Cavitation Research Facilities and Techniques, ASME Publication, New York, May 1964).

11. Thiruvengadam, A. and Preiser, H. S., "On Testing Materials for Cavitation Damage Resistance," HYDRONAUTICS, Incorporated Technical Report 233-3, October 1963. (See also Jour. Ship Research, Vol. 8, No. 3, December 1964).

12. Eisenberg, P., Preiser, H. S., and Thiruvengadam, A., "On the Mechanisms of Cavitation Damage and Methods of Protection," Trans. SNAME, Vol. 73, 1965.

13. Plesset, M. S., and Devine, R. E., "Effect of Exposure Time on Cavitation Damage," Trans. ASME, Jour. Basic Engr., December 1966.

14. Hobbs, J. M., "Experience with a 20 kc/s Cavitation Erosion Test," Symp. on Erosion by Cavitation or Impingement, ASTM Annual Meeting, Atlantic City, June 1966.

15. Smith, A., Kent, R. P., and Armstrong, R. L., "Erosion of Steam Turbine Blade Shield Materials," Symp. on Erosion by Cavitation or Impingement, ASTM Annual Meeting, Atlantic City, June 1966 (See also Proc. Discussion on Deformation of Solids by the Impact of Liquids, Phil. Trans. Royal Society of London, Vol. 260, July 1966, p. 209).

16. Baker, D.W.C., Jolliffe, K. H., and Pearson, D., "The Resistance of Materials to Impact Erosion Damage," Ibid., p. 193.

17. Marriott, J. B., and Rowden, G., "The Erosion of a Cobalt-Chromium Alloy by Liquid Impact," Ibid, p. 144.

18. Busch, H., Hoff, G. and Langbein, G., "Rain Erosion Properties of Materials," Ibid, p. 168 (See also Proc. Symp. Erosion by Cavitation or Impingement, ASTM Special Publication 408, Philadelphia, 1967.

19. Heymann, F. J., "On the Time Dependence of the Rate of Erosion Due to Liquid Impact or Cavitation," Proc. Symp. Erosion by Cavitation or Impingement, ASTM Special Publication 408, Philadelphia, 1967.

20. Cole, R. H., "Under Water Explosions," Princeton University Press, Princeton, New Jersey, 1948.

21. Weibull, W., "Fatigue Testing and Analysis of Results," Pergamon Press, New York, 1961.

22. A Guide for Fatigue Testing and the Statistical Analysis of Fatigue Data (Supplement to Manual on Fatigue Testing, STP No. 91) ASTM Special Technical Publication No. 91-A (Second Edition, Philidelphia, 1963).

23. Manson, S. S., "Fatigue - A Complex Subject - Some Simple Approximations," The William M. Murray Lecture, Experimental Mechanics, Vol. 5, No. 7, July 1965, pp. 193-226.

24. Engel, O. G., Written discussion of Heymann's paper, Reference 19 of this report, 1966. See also Proc. Turbine Erosion Conference, Jet Propulsion Laboratory, 1967.

25. Swanson, S. R., "A Two-Distribution Interpretation of Fatigue S-N Data," Canadian Aeronautical Journal, Vol. 6, No. 6, June 1960.

26. Heymann, F. J., "A Survey of Clues to the Relationship Between Erosion Rate and Impingement Conditions," Proc. Second Meersburg Conference on Rain Erosion, August 1967, Published by Royal Aircraft Establishment, Farnborough, England, August 1967.

27. Properties of Some Metals and Alloys, The International Nickel Company, New York, N. Y., p. 16.

28. Pouchot, W. D. (ed.), "Comparison of the Erosion Potential for a Potassium Vapor Turbine and a Cesium Vapor Turbine," Westinghouse Electric Corporation, Astronuclear Laboratory, WANL-TME-1730, February 9, 1968, Contract NAS 7-390.

29. Christie, D. G., Hayward, G. W., "Observation of Events Leading to the Formation of Water Droplets Which Cause Turbine Blade Erosion (Erosion of Steam Turbine Blades), Meeting of the British Royal Society on Deformation of Solids By the Impact of Liquids, May 27, 1965.

30. W. D. Pouchot, "Oral Presentation at the NASA - GE Third Stage Turbine Tear Down Inspection," Cincinnati, Ohio, October 15, 1968.

31. D.W.C. Baker, D. E. Elliott, D. C. Jones, and D. Pearson, The Erosion Resistance of Steam Turbine Blade and Shield Materials, Proc. Second Meersburg Conference on Rain Erosion and Allied Phenomenon, Royal Aircraft Est. Farnborough, England, August 1967.

32. G. Gyarmathy, "The Bases for a Theory of the Wet Steam Turbine Juris-Verlag, Zurich, 1962, also published in Bull. No. 6, Inst. for Thermal Turbo Fuel Machines on Fed. Tech. University, Zurich, Switzerland.

33. A. A. Fyall, R. B. King, and R.N.C. Strain, "Rain Erosion Aspects of Aircrafts and Guided Missiles," Jour. Royal Aeronautical Society, 1962, p. 467.

34. G. Hoff, G. Langbein and H. Rieger, "Material Destruction Due to Liquid Impact," Erosion by Cavitation or Impingement, STP 408 American Society for Testing and Materials, 1967.

35. Sajben, M., "Description of Moisture Erosion on Turbine Blades with Comparative Photographs, Westinghouse Steam Div., Report EM-437, December 1959.

36. A. P. Fraas, H. C. Young and A. G. Grindell, Survey of Information on Turbine Bucket Erosion, DRNL-TM-2088, Oak Ridge National Lab., Oak Ridge, Tenn., July 1968.

37. S. G. Young and J. R. Johnston, "Accelerated Cavitation Damage of Steels and Superalloys in Sodium and Mercury," Erosion by Cavitation or Impingement, ASTM STP-408, Am. Soc. Testing Mats., 1967, p.186-212.

TABLE 1

Multiple Liquid Impact Erosion Strength

Diameter of Water Jet 1/32 Inch. Specimen Diameter 3/8 inch.

Water Temperature 68°F.

Strain Energy of Commercially Pure Nickel = 20,000 psi

Material	Velocity fps	Maximum Erosion Rate cc/hr	Erosion Strength, psi	Remarks
Nickel B-160	350	3.5×10^{-3}	20,000	
Stainless Steel	350	2.0×10^{-3}	35,000	I = 18 watts/sq.m.
Titanium (6 Al-4V)	350	0.4×10^{-3}	175,000	(See text pg. 26)
Aluminum 1100-0	350	70×10^{-3}	1,000	

Note: All the metals were annealed before machining.
The 316 SS is cold drawn 3/8 rod.

TABLE 2

Cavitation Erosion Strength

Specimen Diatermeter 3/8 Inch. Magnetostriction Vibratory Apparatus
Distilled Water at 68°F.
Strain Energy of Commercially Pure Nickel: 20,000 psi
Double Amplitude: 3×10^{-3} in. Frequency 13.5 kc

Material	Maximum Erosion Rate, cc/hr	Erosion Strength, psi	Remarks
Nickel B-160	2.8×10^{-3}	20,000	
Stainless Steel 316	1.0×10^{-3}	56,000	
Titanium (6 Al-4V)	0.9×10^{-3}	62,000	I_e = 2.5 w/sq.m.
Aluminum 1100-0	100×10^{-3}	6,000	(See text pg. 26)

Note: All metals were annealed before machining.
The 316 SS is cold drawn 3/8 rod.

TABLE 3

Properties of Water, Potassium and Cesium (Reference 28)

	Density (ρ)		Speed of Sound (C)	ρC	Relative ρC
	lbs/cft	Slugs / cft	ft/sec	Slugs / ft^2/sec	as compared to water %
Water @ Room Temp	62.4	1.94	4800	9300	100
Potassium @ 1200°F	43.1	1.34	4923	6600	71
Potassium @ 1300°F	42.3	1.31	4833	6300	68
Cesium @ 1200°F	93	2.88	2400	6900	74
Cesium @ 1300°F	91	2.82	2300	6500	70

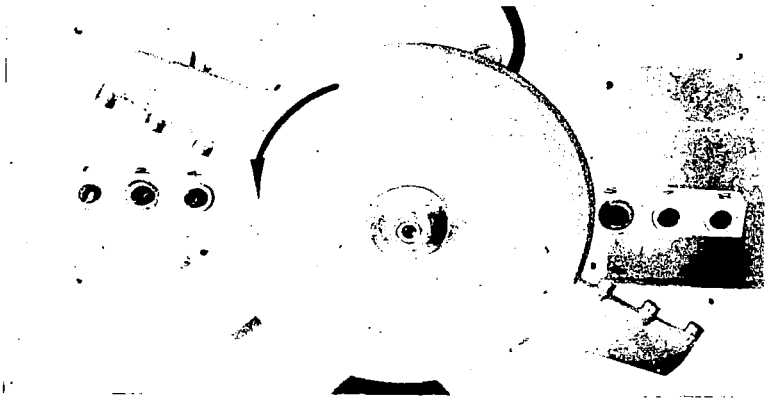

ROTATING DISC

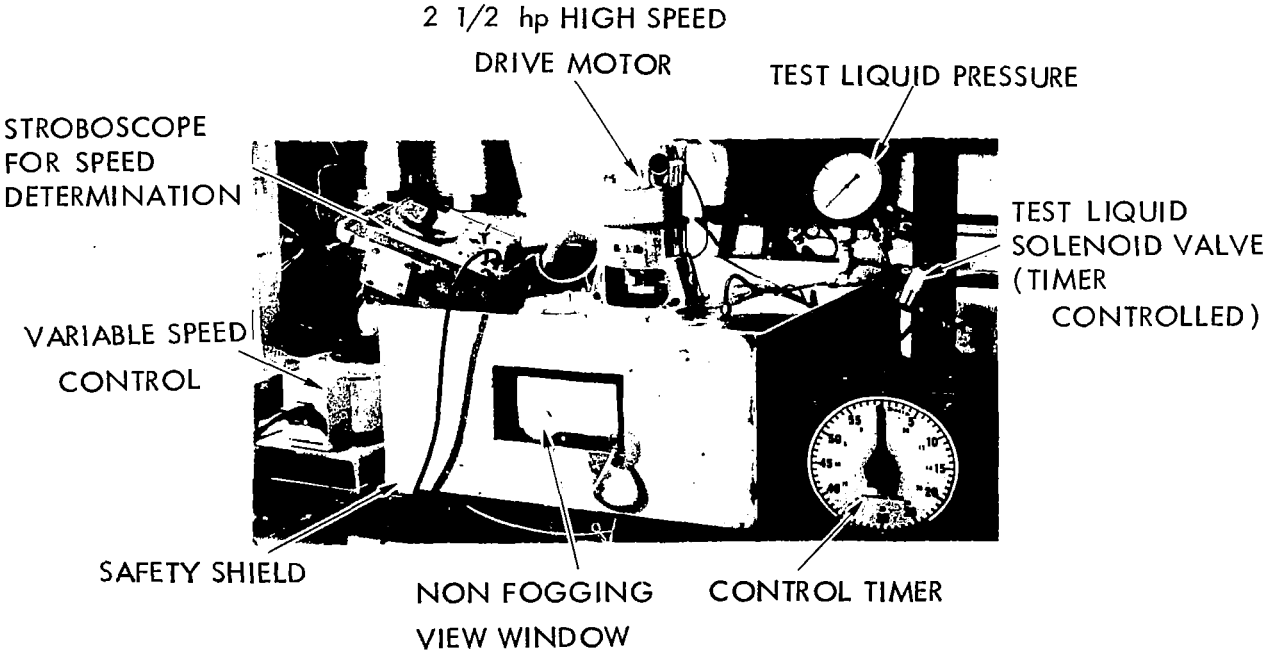

FIGURE 1 - GENERAL VIEW OF HYDRONAUTICS JET IMPACT EROSION FACILITY

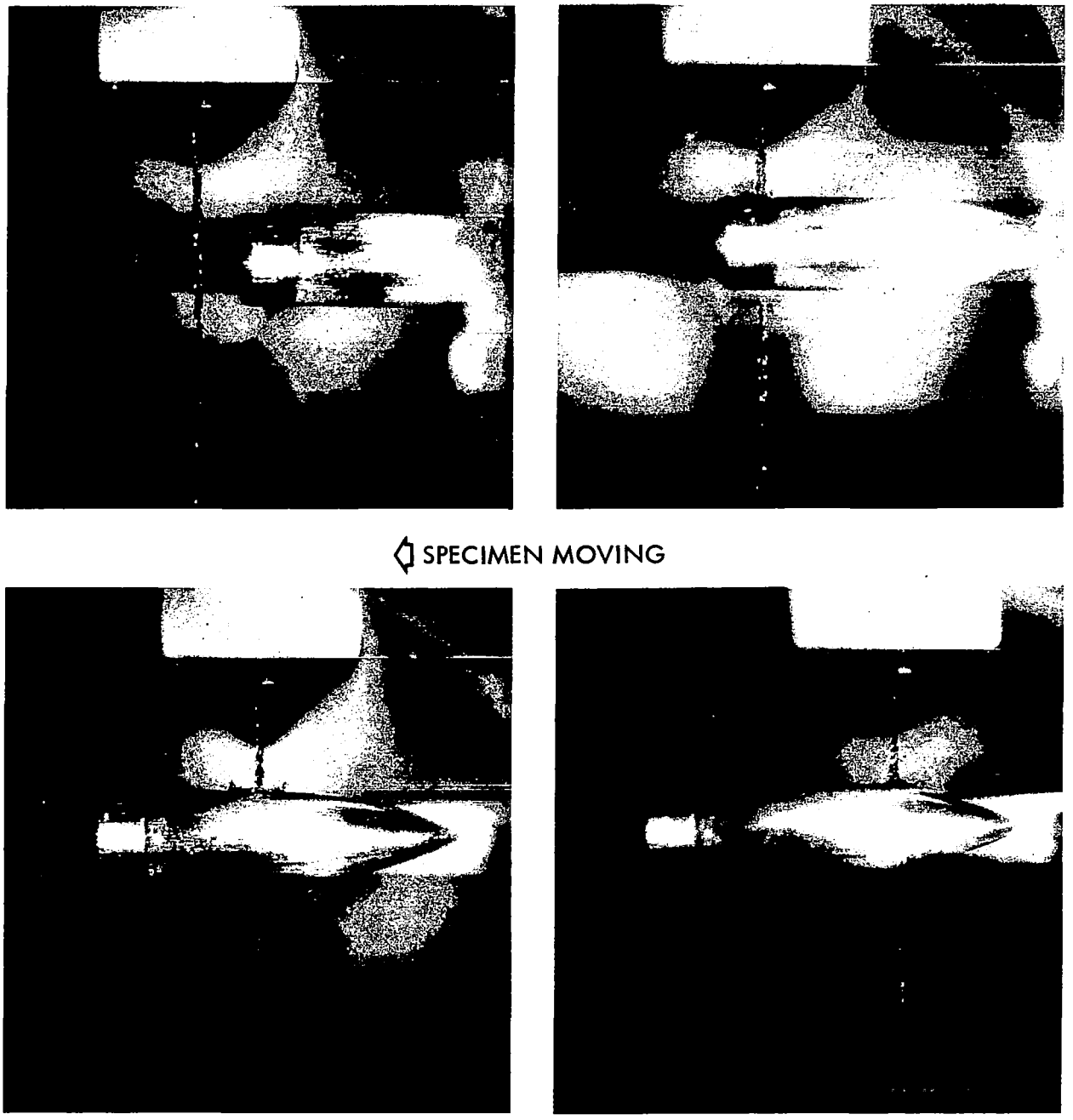

FIGURE 2 - TYPICAL WATER COLUMN AND SPRAY PATTERN DURING SPECIMEN PROGRESSION

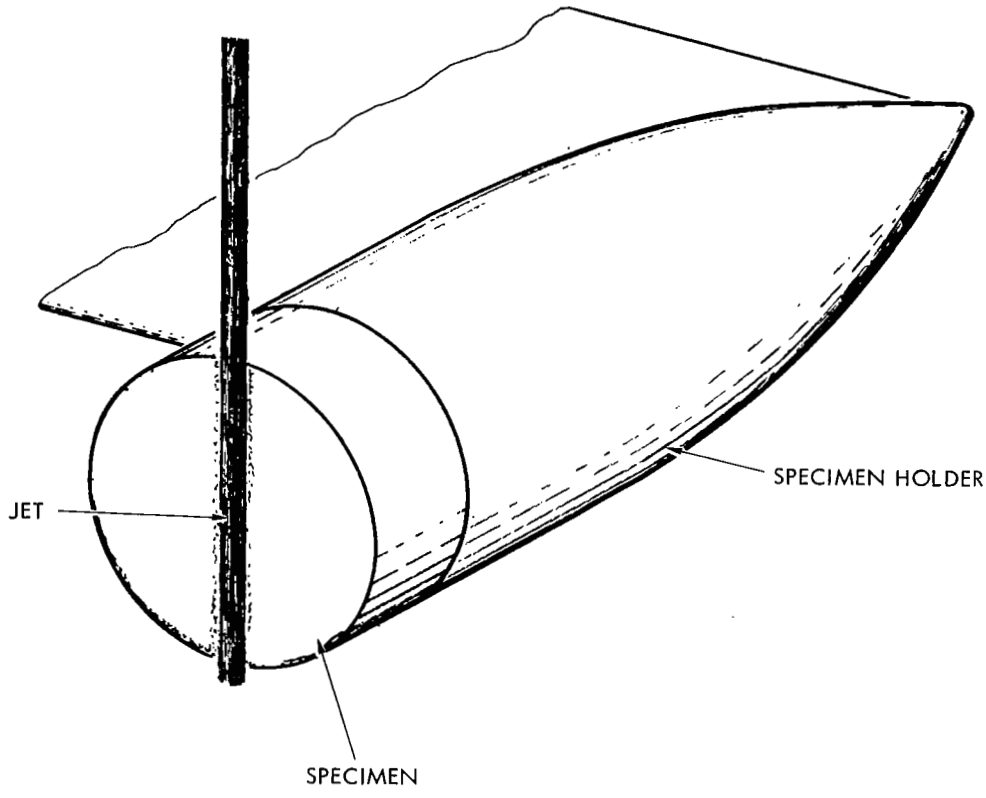

IMPACT OF LIQUID JET BY TEST SPECIMEN

FIGURE 2 a

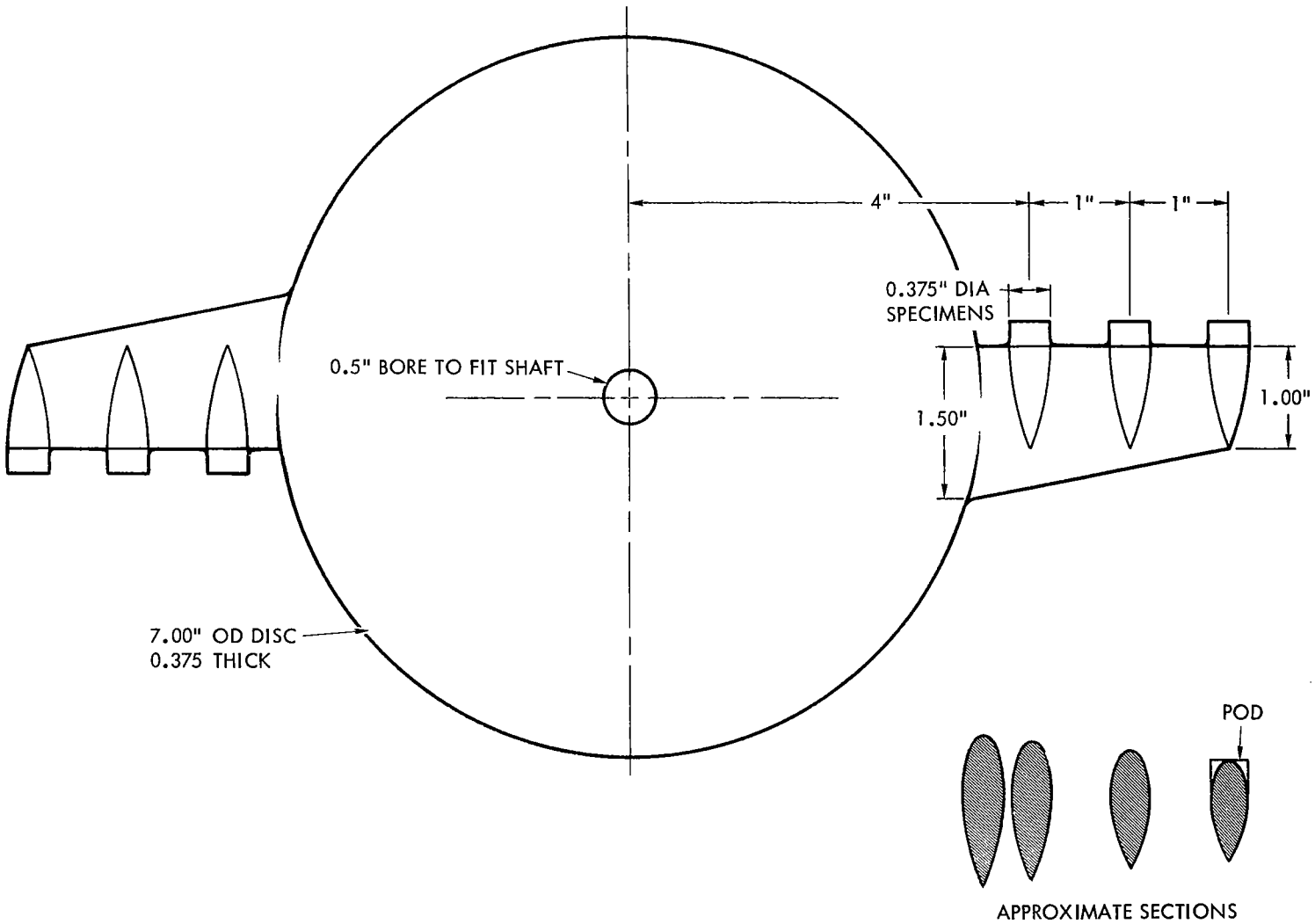

FIGURE 3 - ROTATING DISC CAPABLE OF HOLDING SIX SPECIMENS

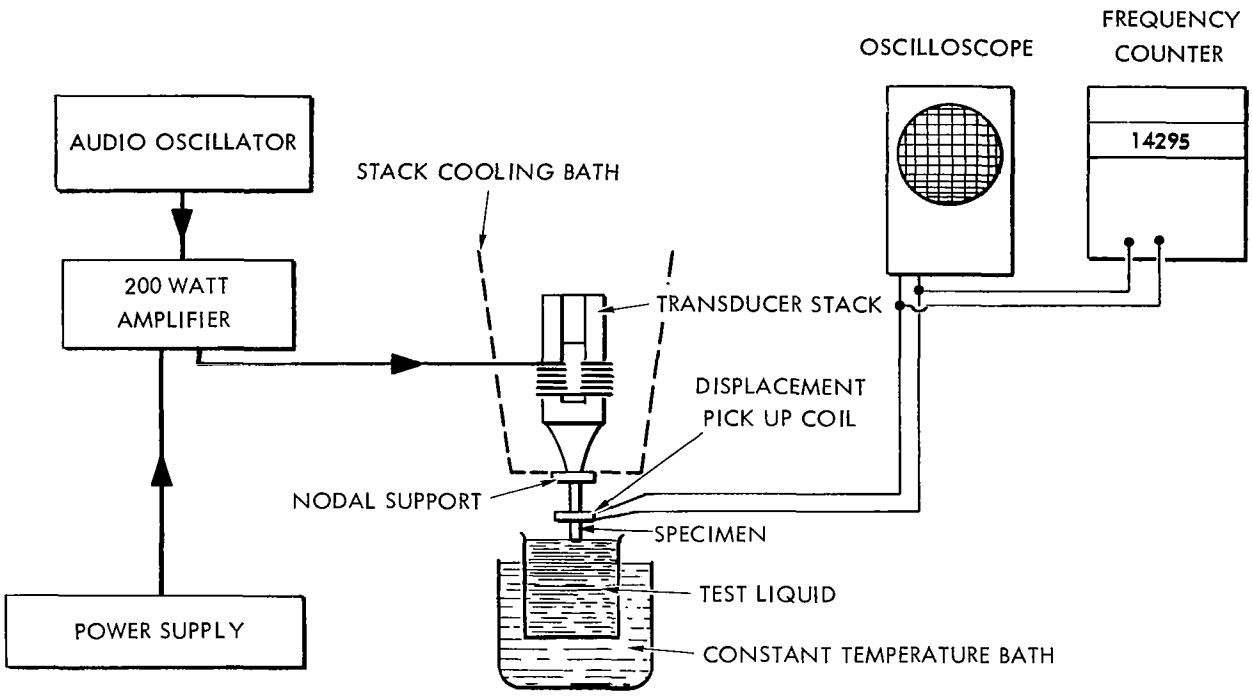

FIGURE 4 - BLOCK DIAGRAM OF THE MAGNETOSTRICTION APPARATUS USED FOR HIGH FREQUENCY FATIGUE TESTS

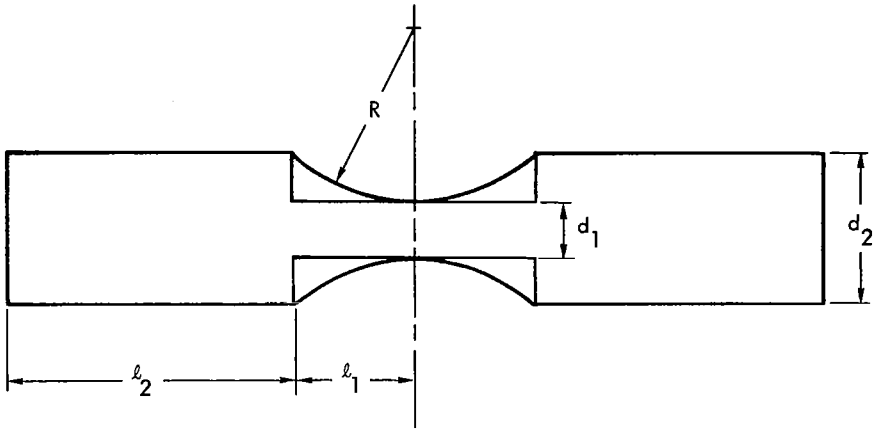

$$\left(\frac{d_2}{d_1}\right)^2 = \text{AREA RATIO}$$

$\frac{\ell_1}{\lambda}$ AND $\frac{\ell_2}{\lambda}$ ARE RELATIVE LENGTHS

WHERE λ = WAVE LENGTH OF THE MATERIAL FOR THE TEST FREQUENCY

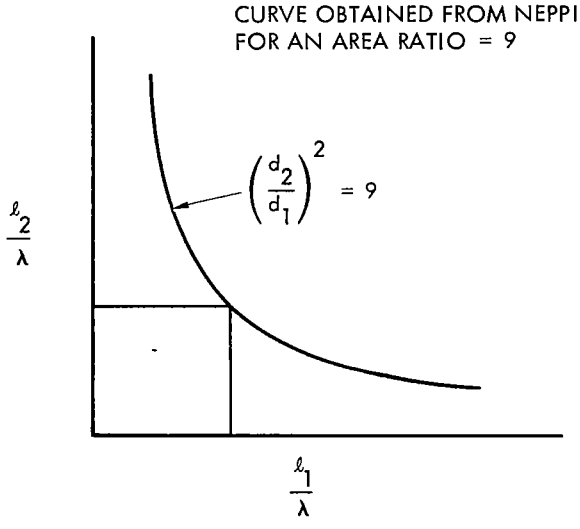

FIGURE 5 - BASIC APPROACH FOR THE DESIGN OF DUMB-BELL SHAPED FATIGUE SPECIMENS

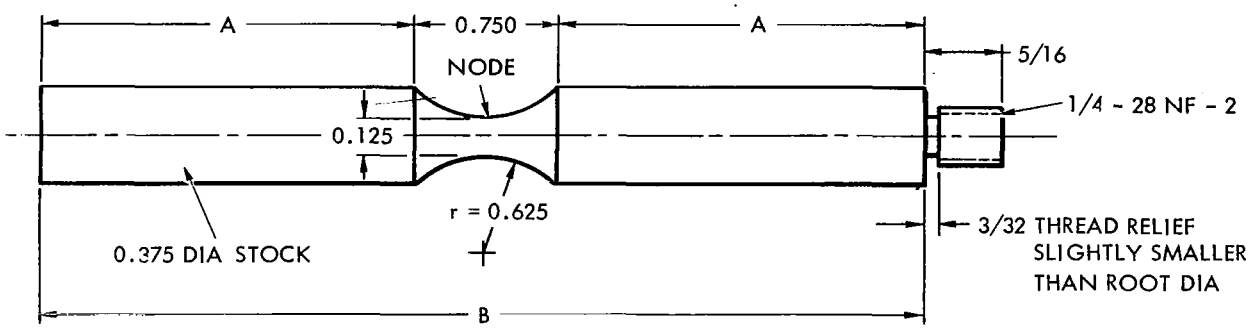

DECIMALS	±0.001
FRACTIONS	±0.010
FINISH	# 125 UNLESS NOTED

NOTE: 0.625 r REDUCED AREA TO BE GROUND AND POLISHED TO 32 RMS MINIMUM

ALL DIMENSIONS ARE IN INCHES

TYPICAL ROOM TEMPERATURE DIMENSIONS

MATERIAL	DIMENSION A	DIMENSION B
316 STAINLESS STEEL	1.812	4.375
1100-0 ALUMINUM	1.855	4.460
99.57 %NICKEL	1.784	4.318
TITANIUM 6AL - 4V	1.845	4.440

FIGURE 6 - DUMB-BELL SHAPED HIGH FREQUENCY FATIGUE SPECIMEN

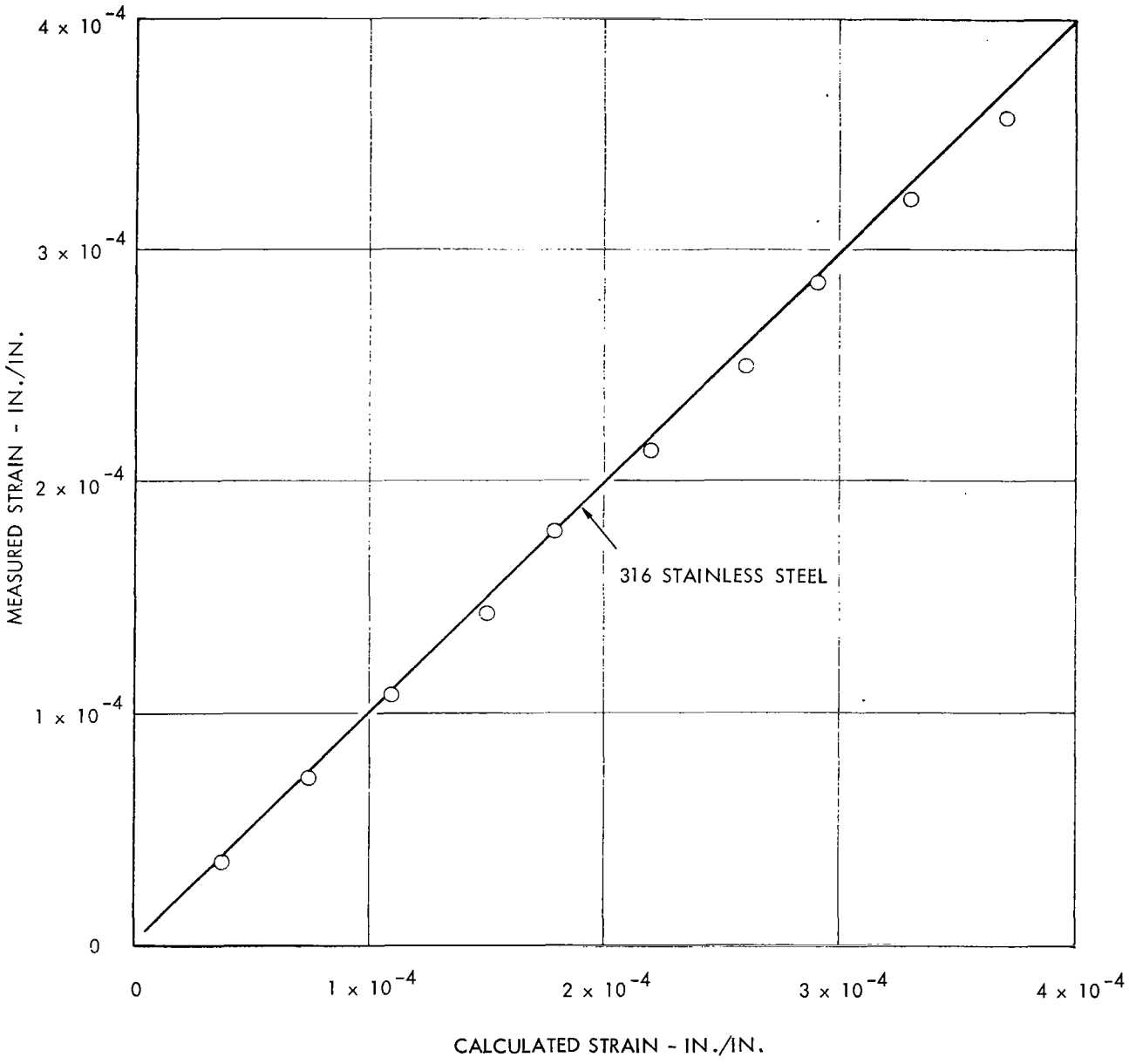

FIGURE 7 - COMPARISON OF THEORETICAL STRAIN AND MEASURED STRAIN FOR DUMB-BELL SHAPED FATIGUE SPECIMENS

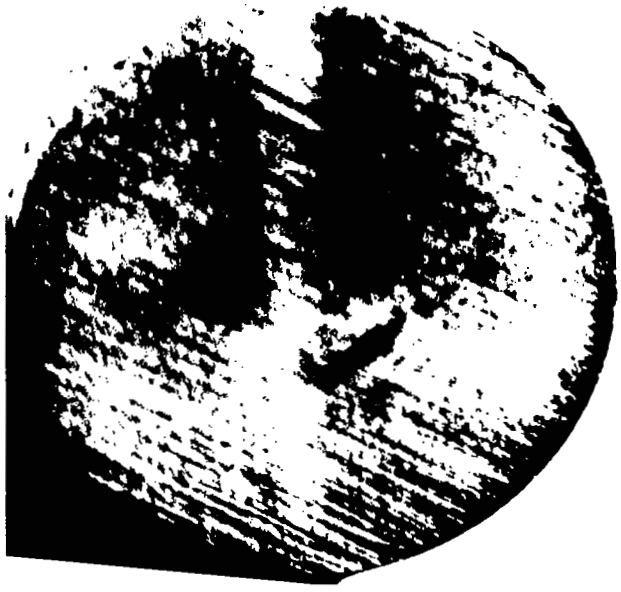

FIGURE 8 - 316 STAINLESS STEEL SPECIMEN RUN 20 HOURS AT 150 FT/SEC FOR 8.3×10 IMPACTS TO THRESHOLD.

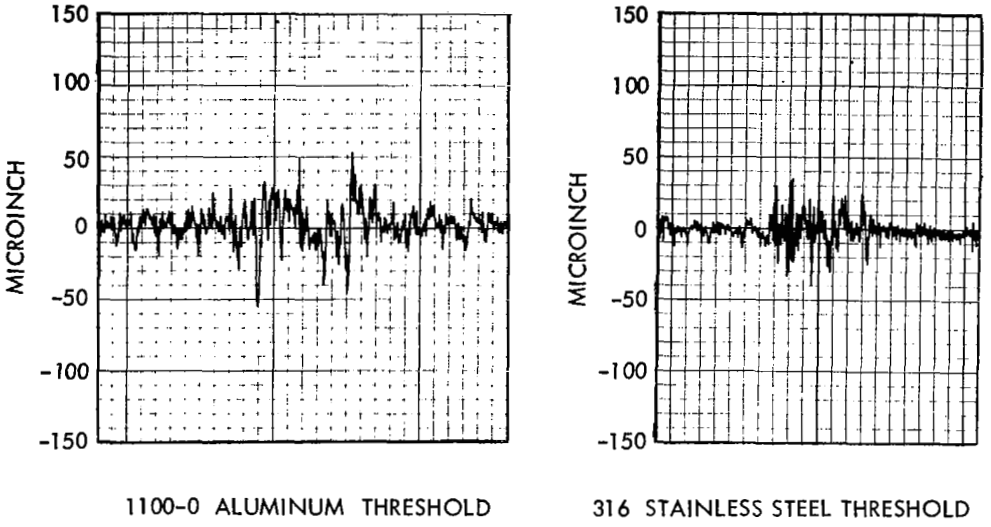

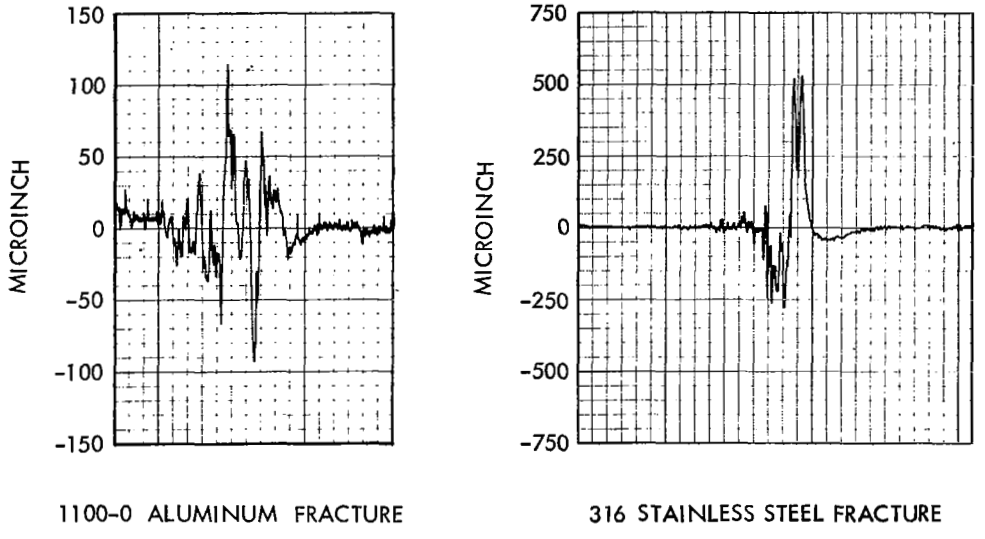

FIGURE 9 - SURFACE ROUGHNESS PROFILE AT THRESHOLD AND AT FRACTURE

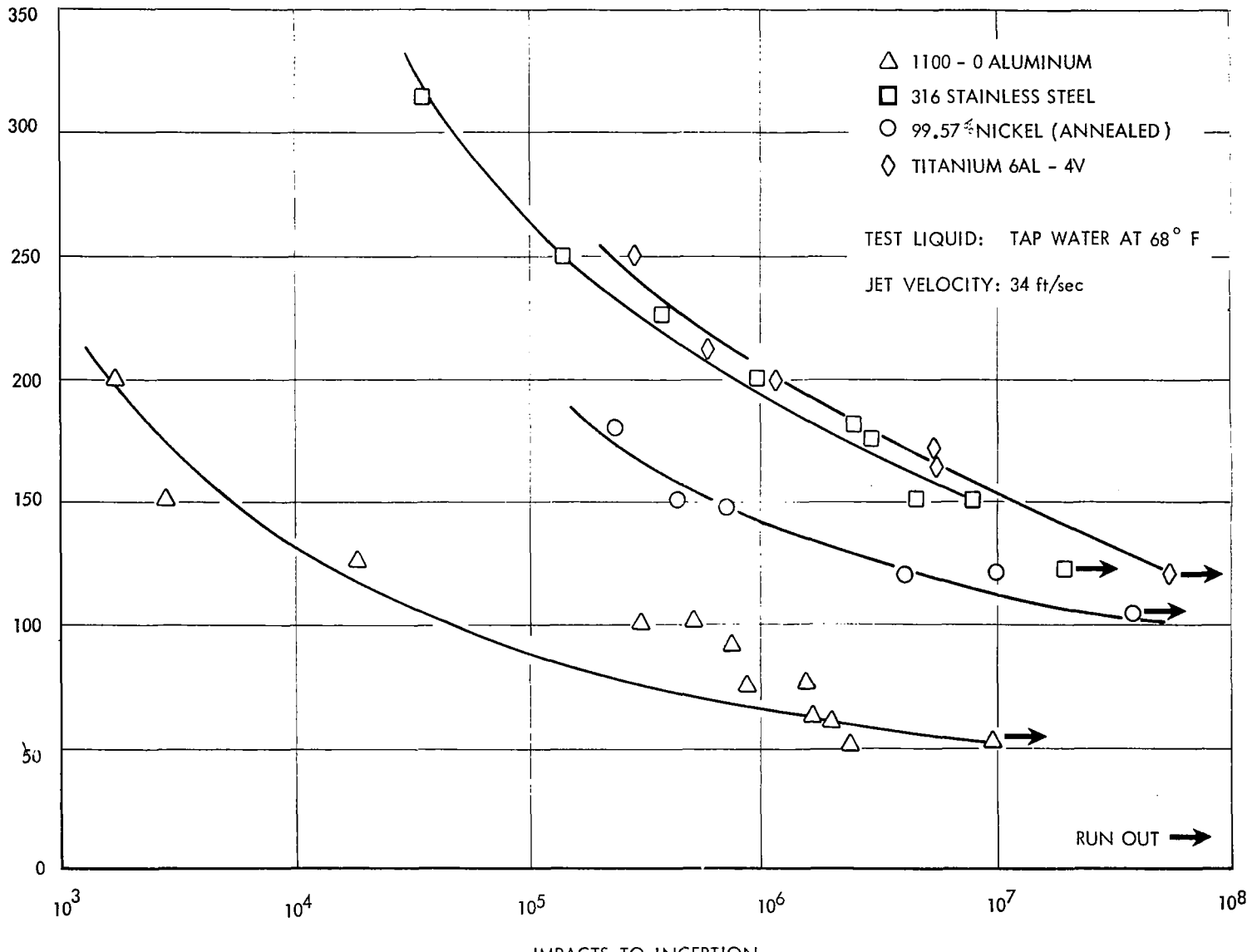

FIGURE 10 - RELATIONSHIP BETWEEN IMPACT VELOCITY AND THE NUMBER OF IMPACTS UNTIL INITIAL PLASTIC DENTS ARE OBSERVED

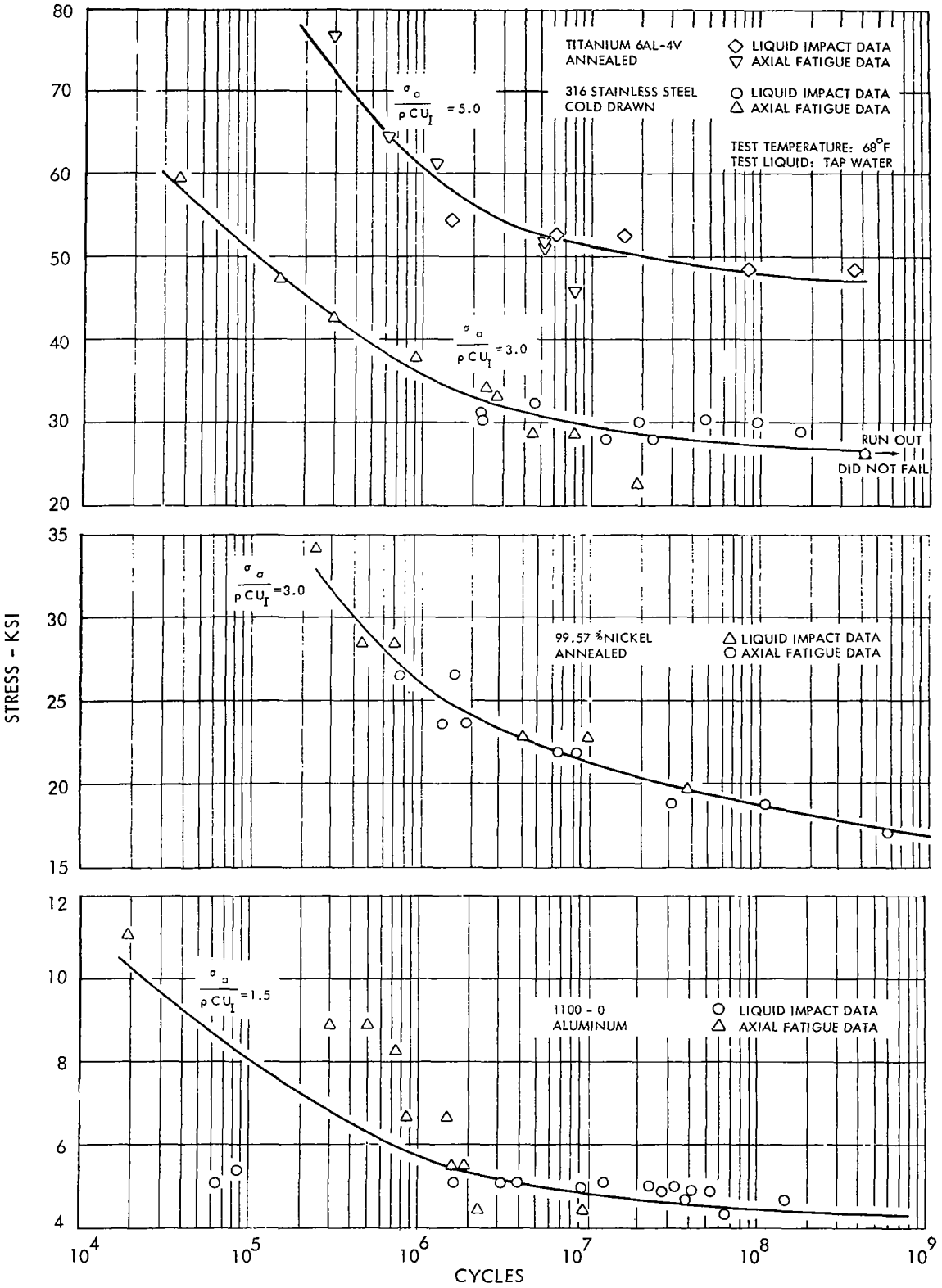

FIGURE 11 - CORRELATION OF WATER HAMMER STRESSES WITH FATIGUE ENDURANCE LIMITS

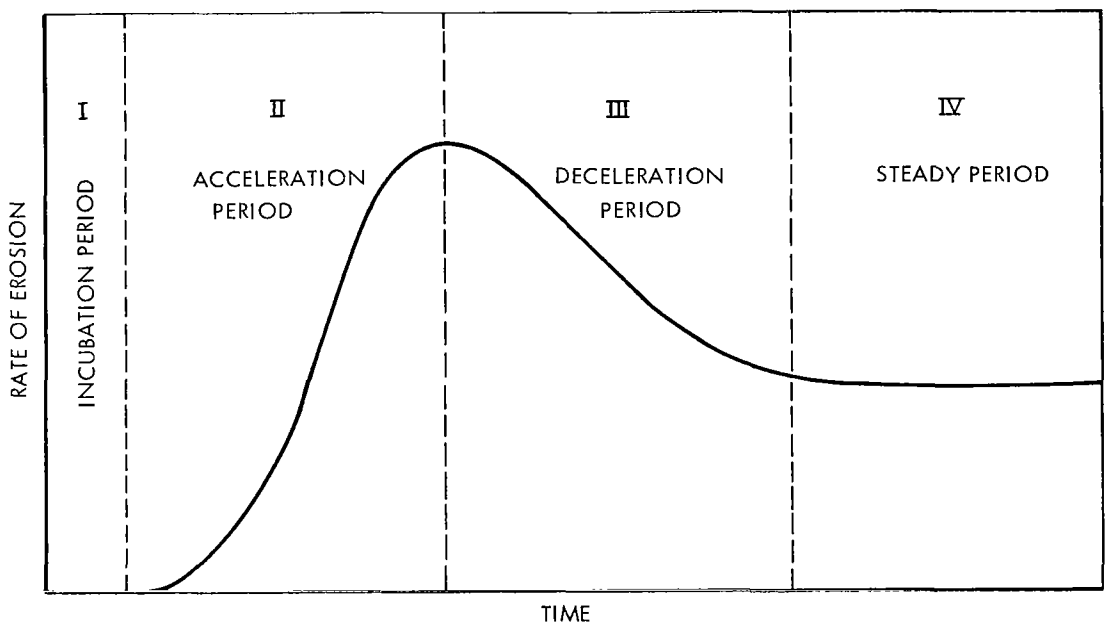

FIGURE 12 - EFFECT OF TIME ON RATE OF EROSION

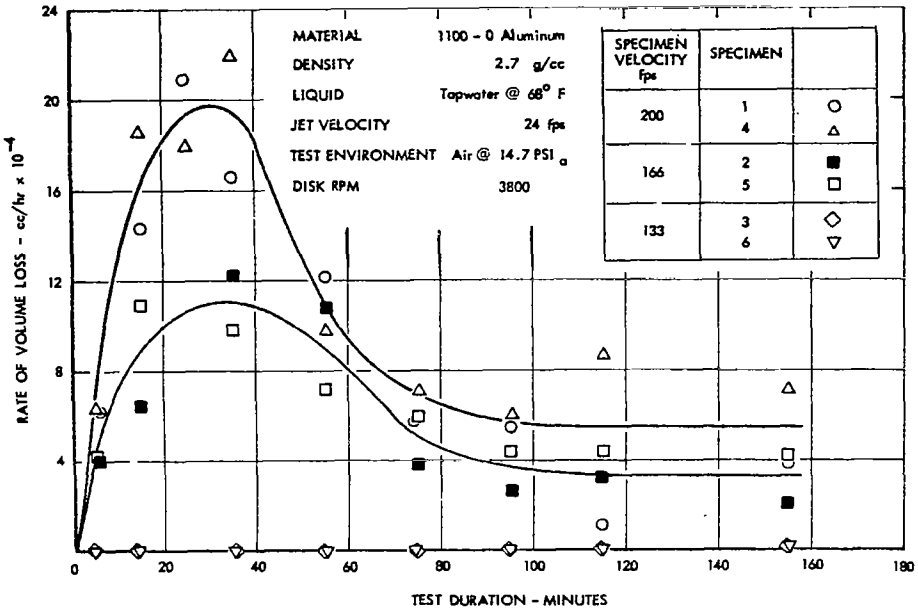

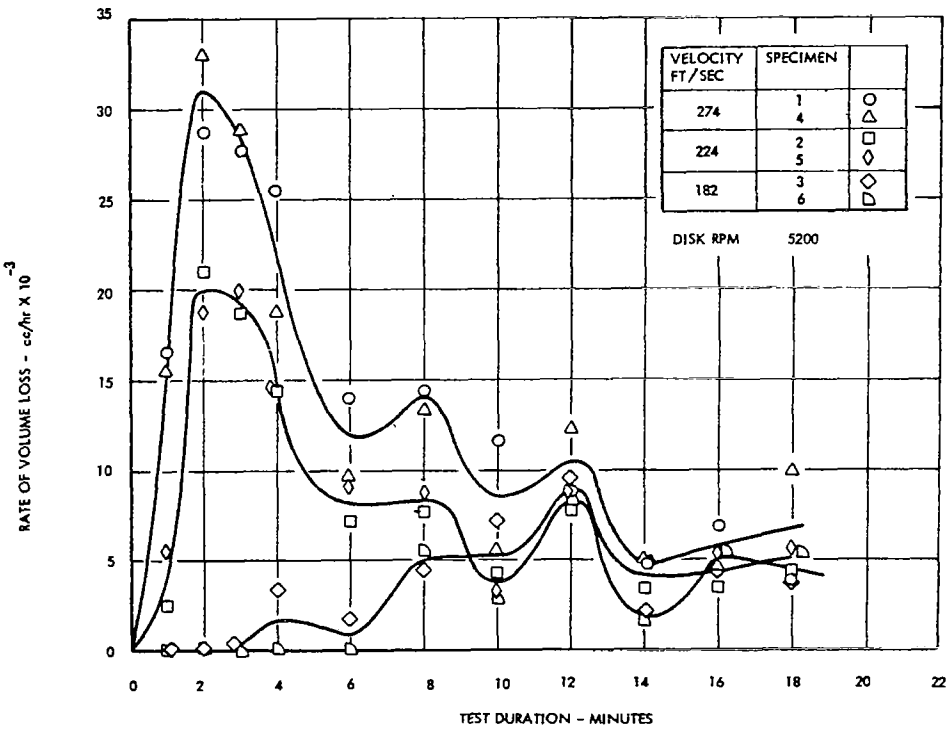

FIGURE 13 - RATE OF VOLUME LOSS AS A FUNCTION OF TIME FOR 1100-0 ALUMINUM

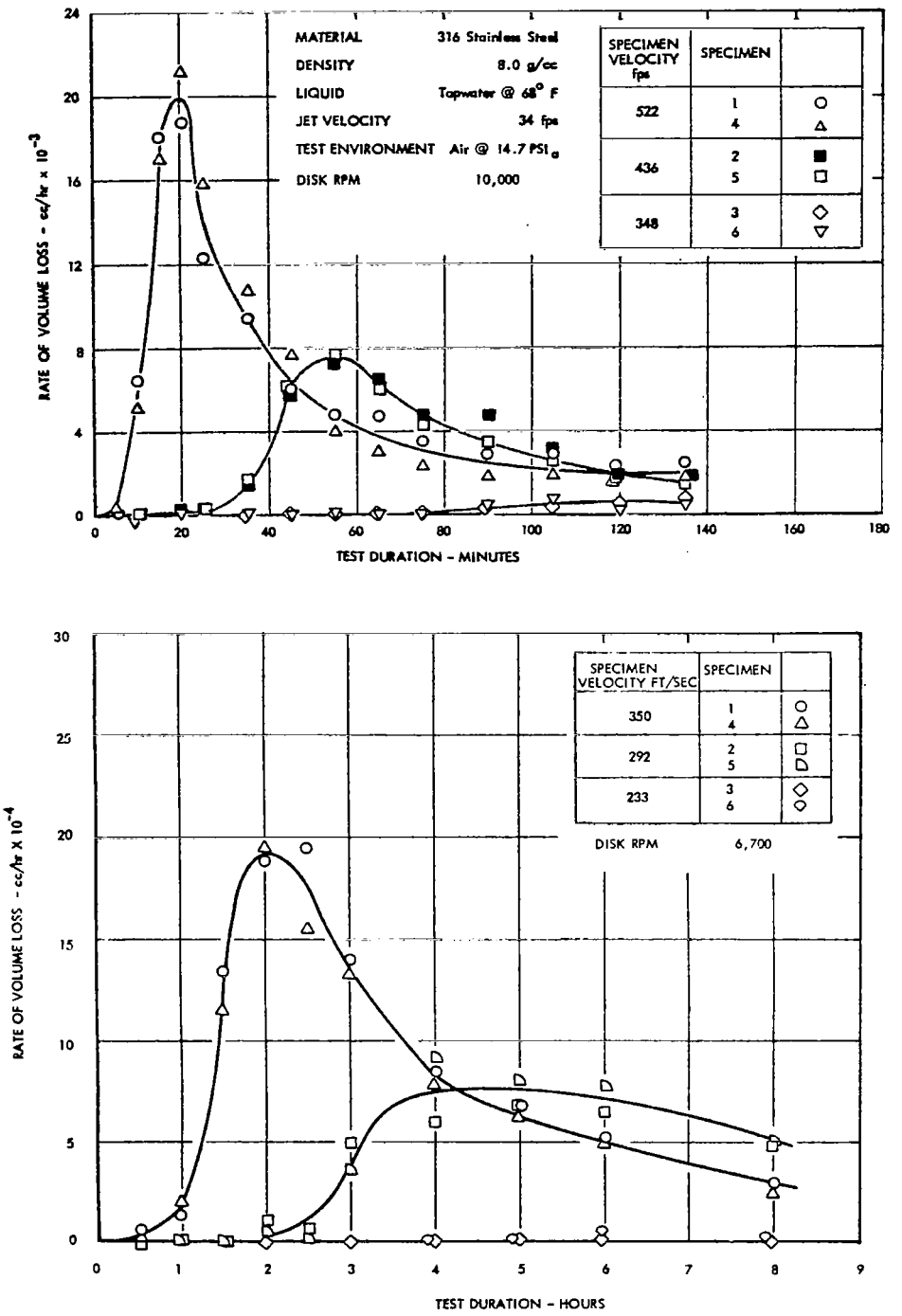

FIGURE 14 - RATE OF VOLUME LOSS AS A FUNCTION OF TIME FOR 316 STAINLESS STEEL (COLD DRAWN)

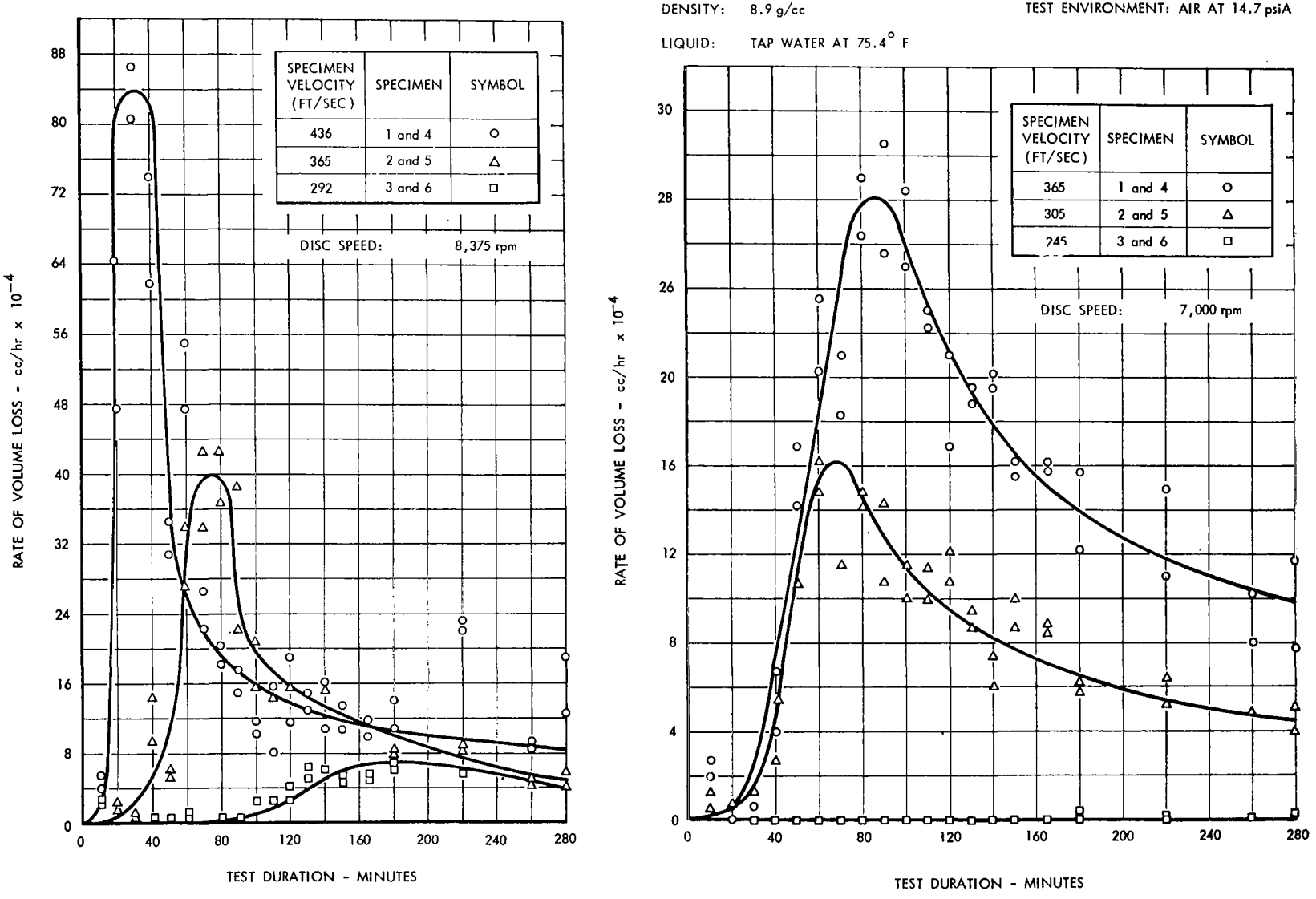

FIGURE 15 - RATE OF VOLUME LOSS AS A FUNCTION OF TIME FOR 99.57% PURE NICKEL (ANNEALED)

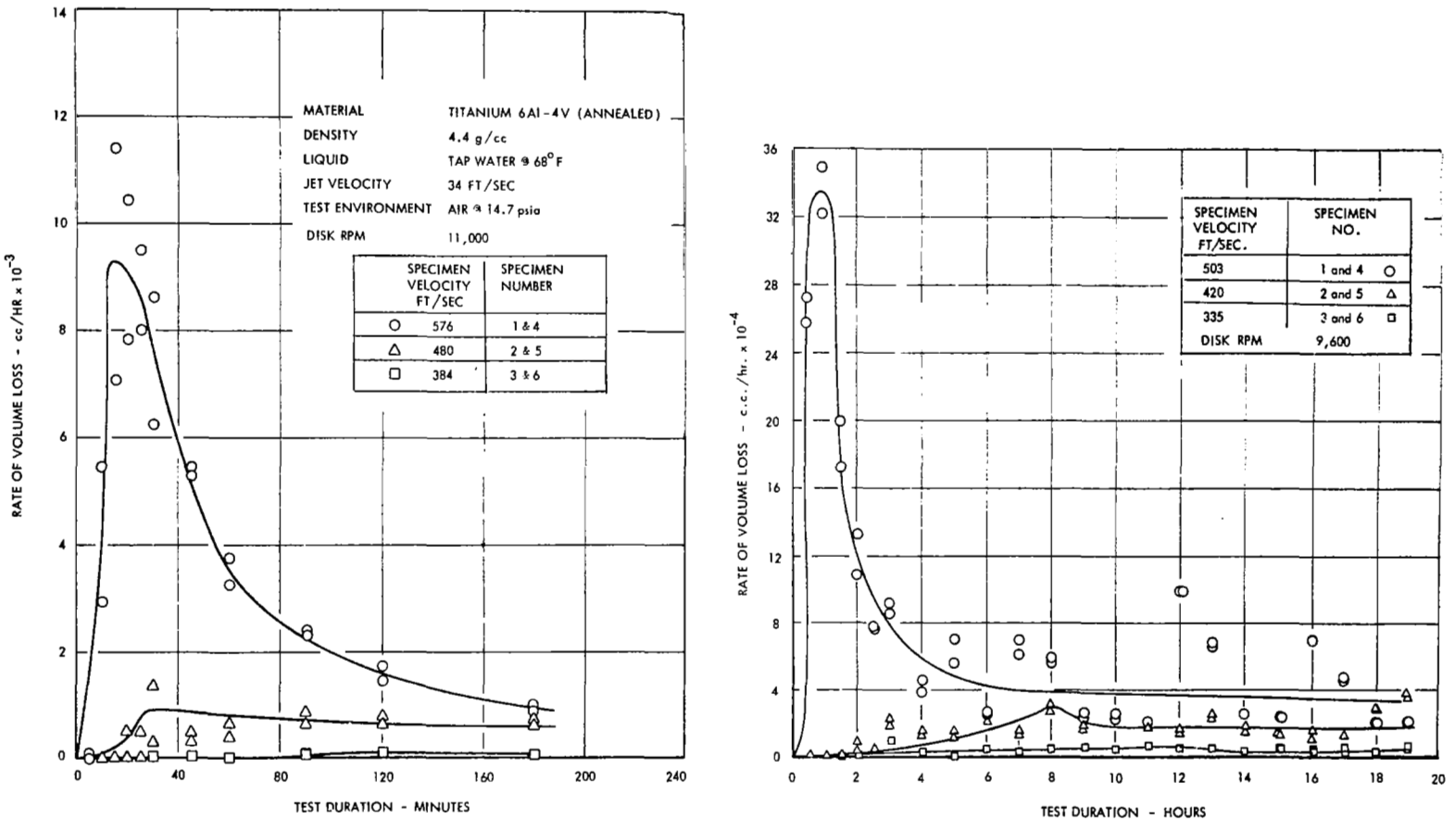

FIGURE 16 - RATE OF VOLUME LOSS AS A FUNCTION OF TIME FOR TITANIUM 6AL-4V (ANNEALED)

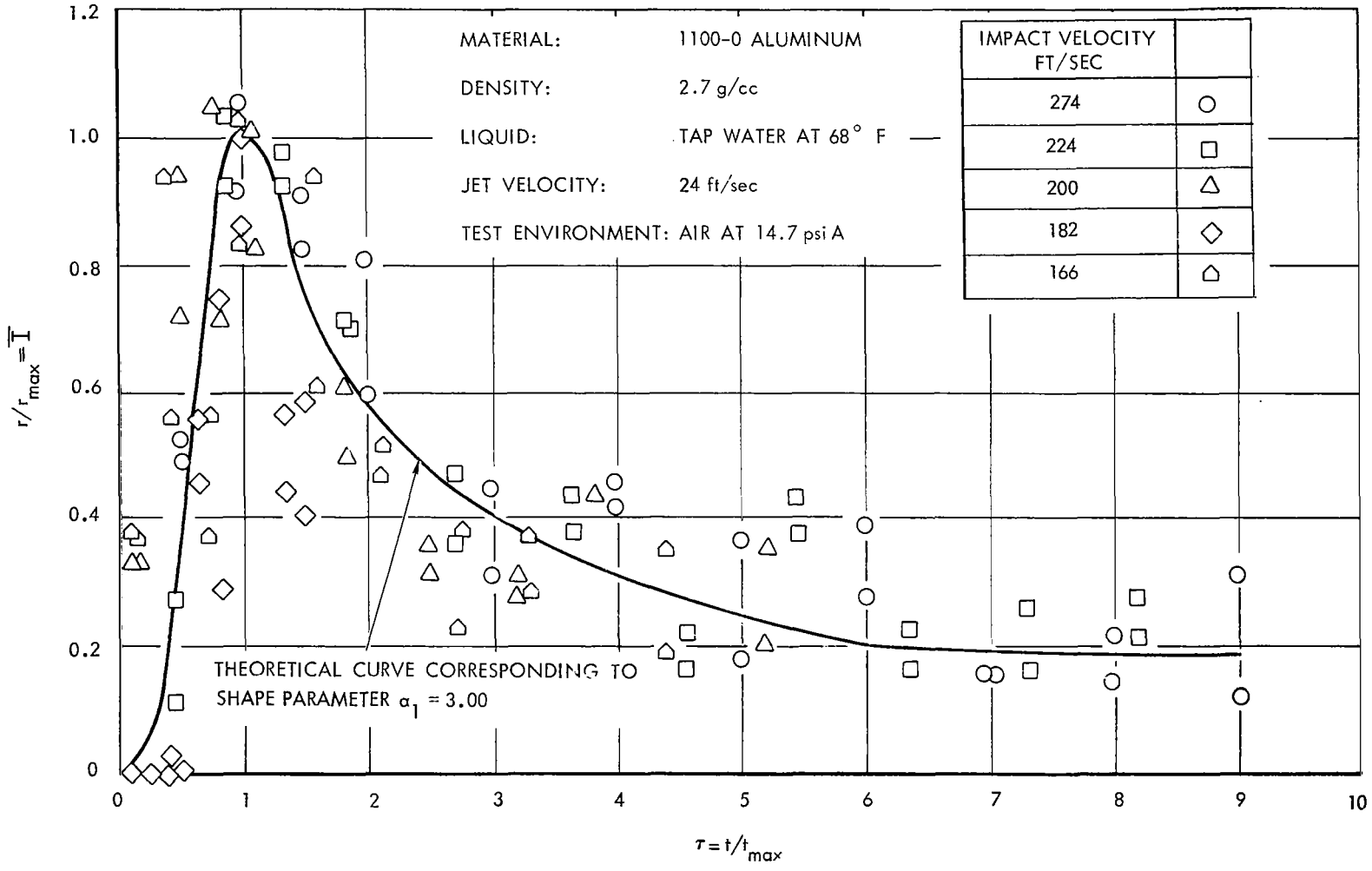

FIGURE 17 - COMPARISON OF EXPERIMENTAL RESULTS WITH THE EROSION THEORY FOR 1100-0 ALUMINUM

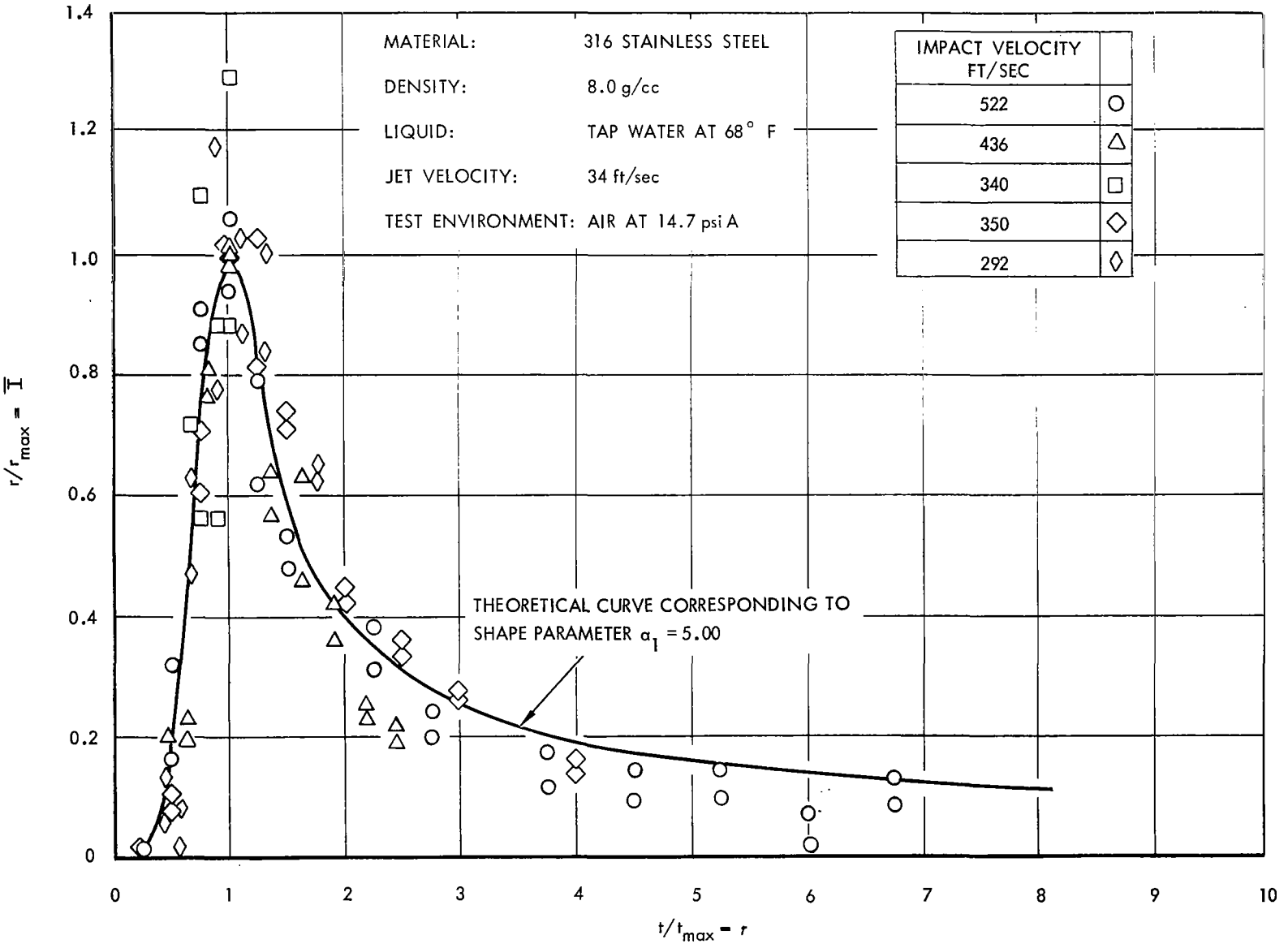

FIGURE 18 - COMPARISON OF EXPERIMENTAL RESULTS WITH THE EROSION THEORY FOR 316 STAINLESS STEEL

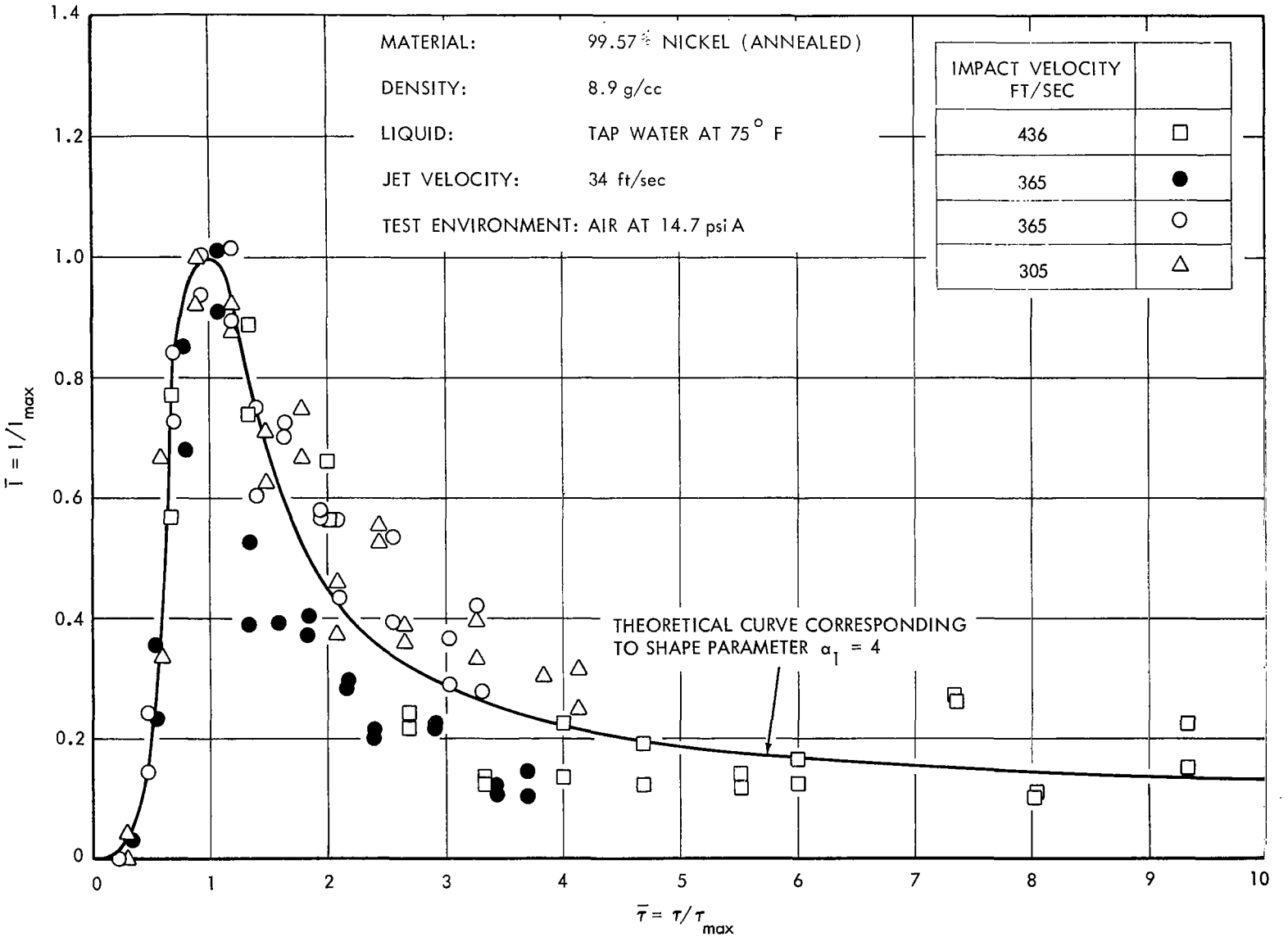

FIGURE 19 - COMPARISON OF EXPERIMENTAL RESULTS WITH THE EROSION THEORY FOR ANNEALED 99.57% NICKEL

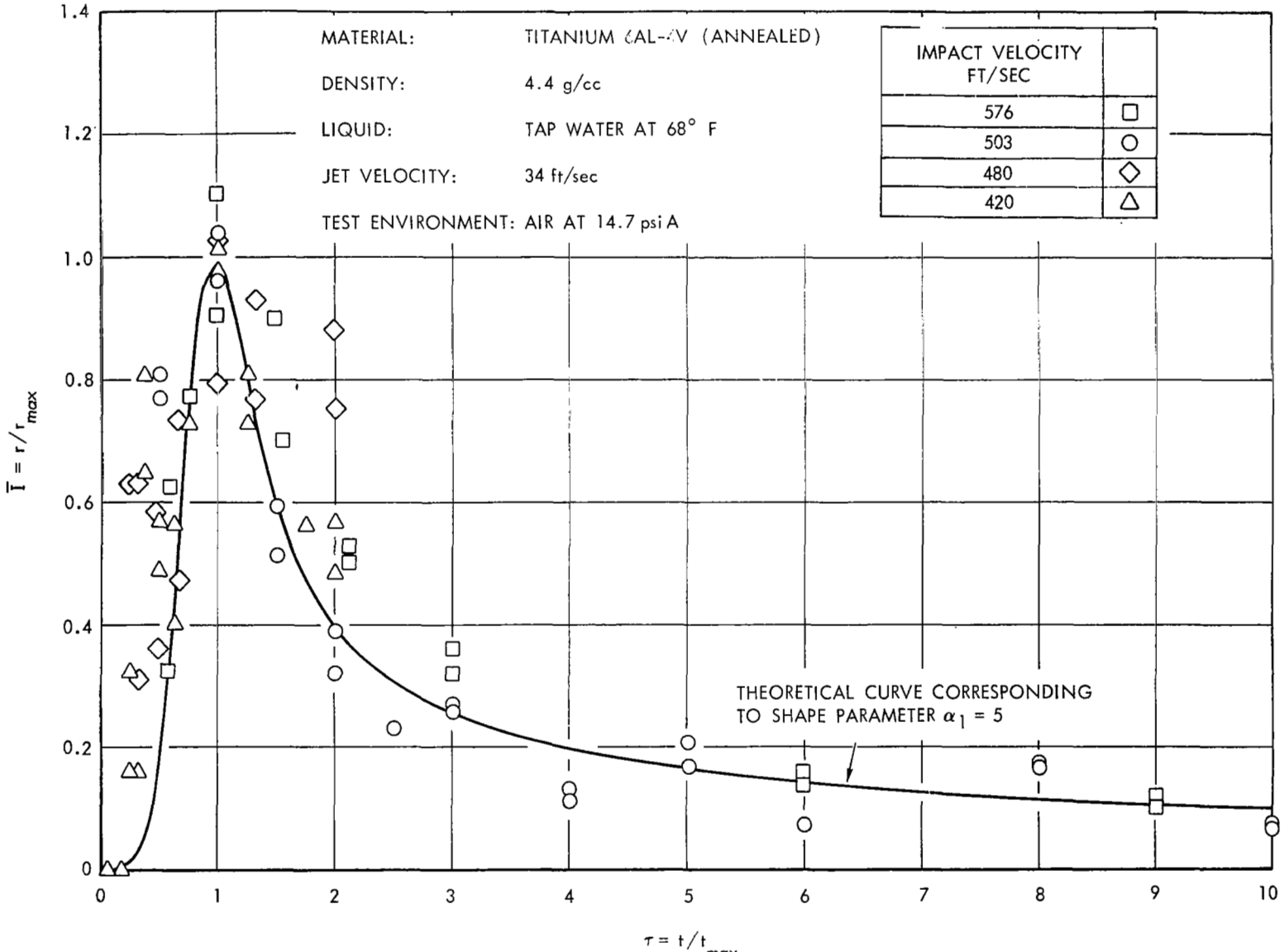

FIGURE 20 - COMPARISON OF EXPERIMENTAL RESULTS WITH THE EROSION THEORY FOR TITANIUM 6AL - 4V

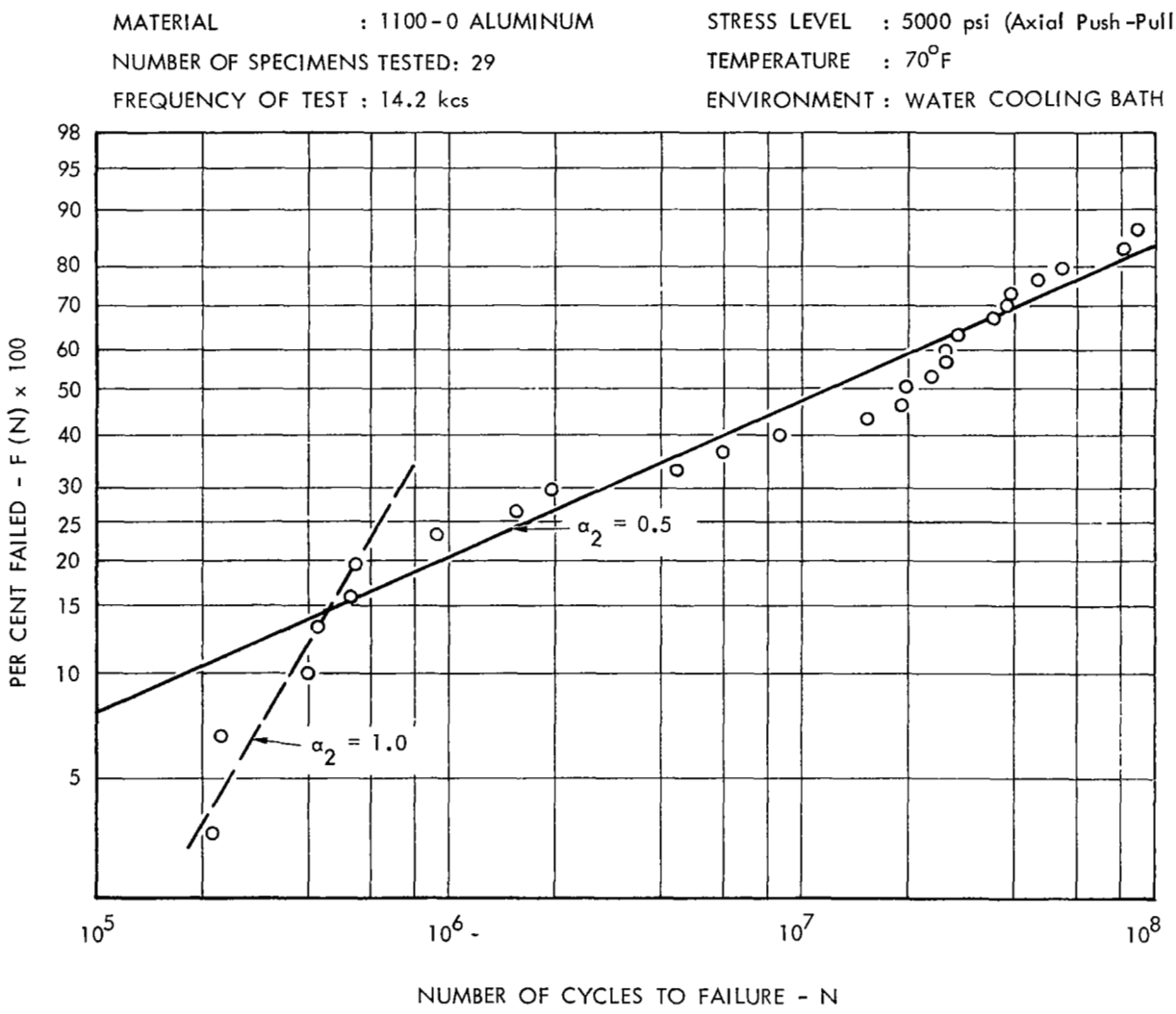

FIGURE 21 - WEIBULL DISTRIBUTION FOR HIGH FREQUENCY FATIGUE OF 1100-0 ALUMINUM

MATERIAL : 316 STAINLESS STEEL

NUMBER OF SPECIMENS TESTED: 20

FREQUENCY OF TEST : 14.2 kcs

STRESS LEVEL : 30,000 psi (Axial Push-Pull)

TEMPERATURE : 70 ° F

ENVIRONMENT : WATER COOLING BATH

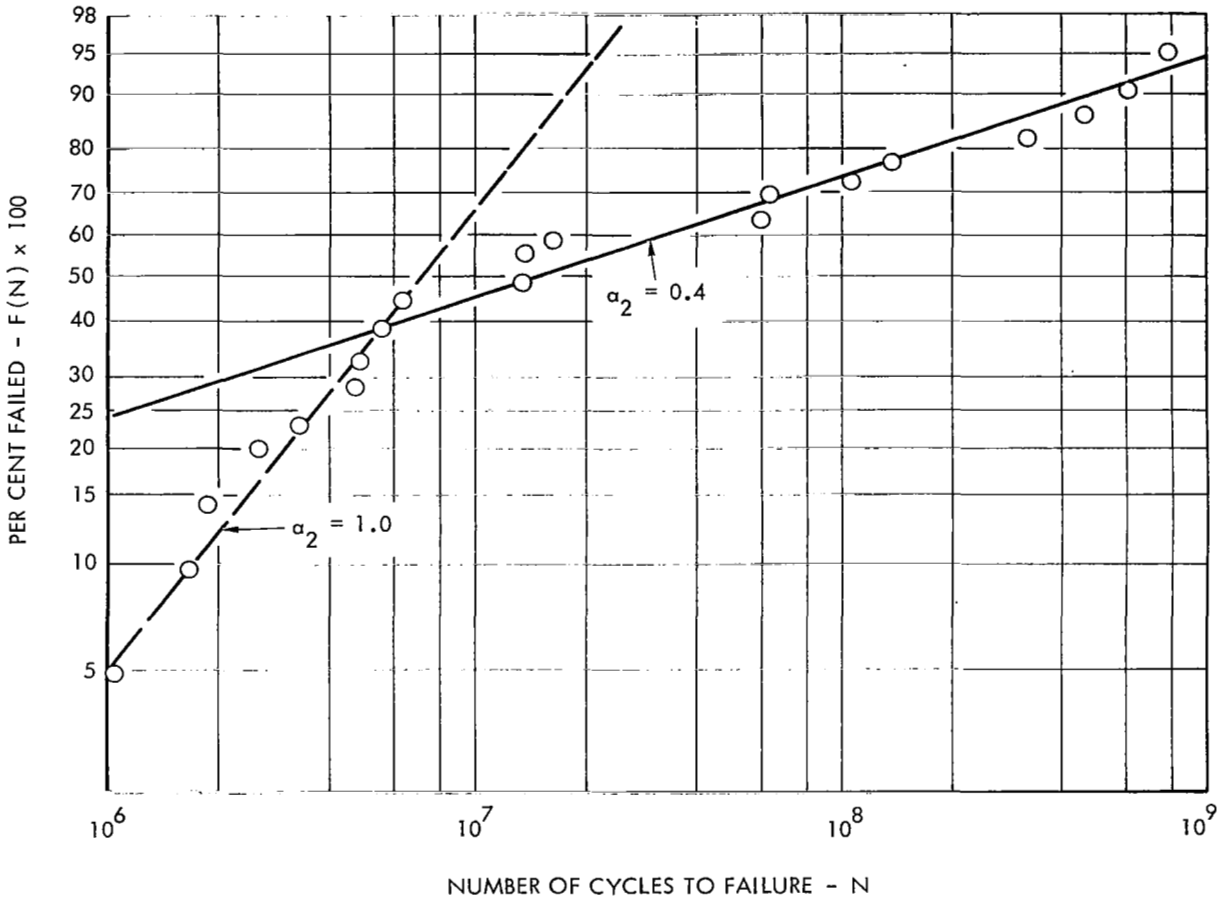

FIGURE 22 - WEIBULL DISTRIBUTION FOR HIGH FREQUENCY FATIGUE OF 316 STAINLESS STEEL

MATERIAL: TITANIUM 6AL - 4V ANNEALED
NUMBER OF SPECIMENS TESTED: 30
FREQUENCY OF TEST: 14.0 kcs

STRESS LEVEL: 52,800 psi (AXIAL PUSH PULL)
TEMPERATURE: 70°F
ENVIRONMENT: WATER COOLING BATH

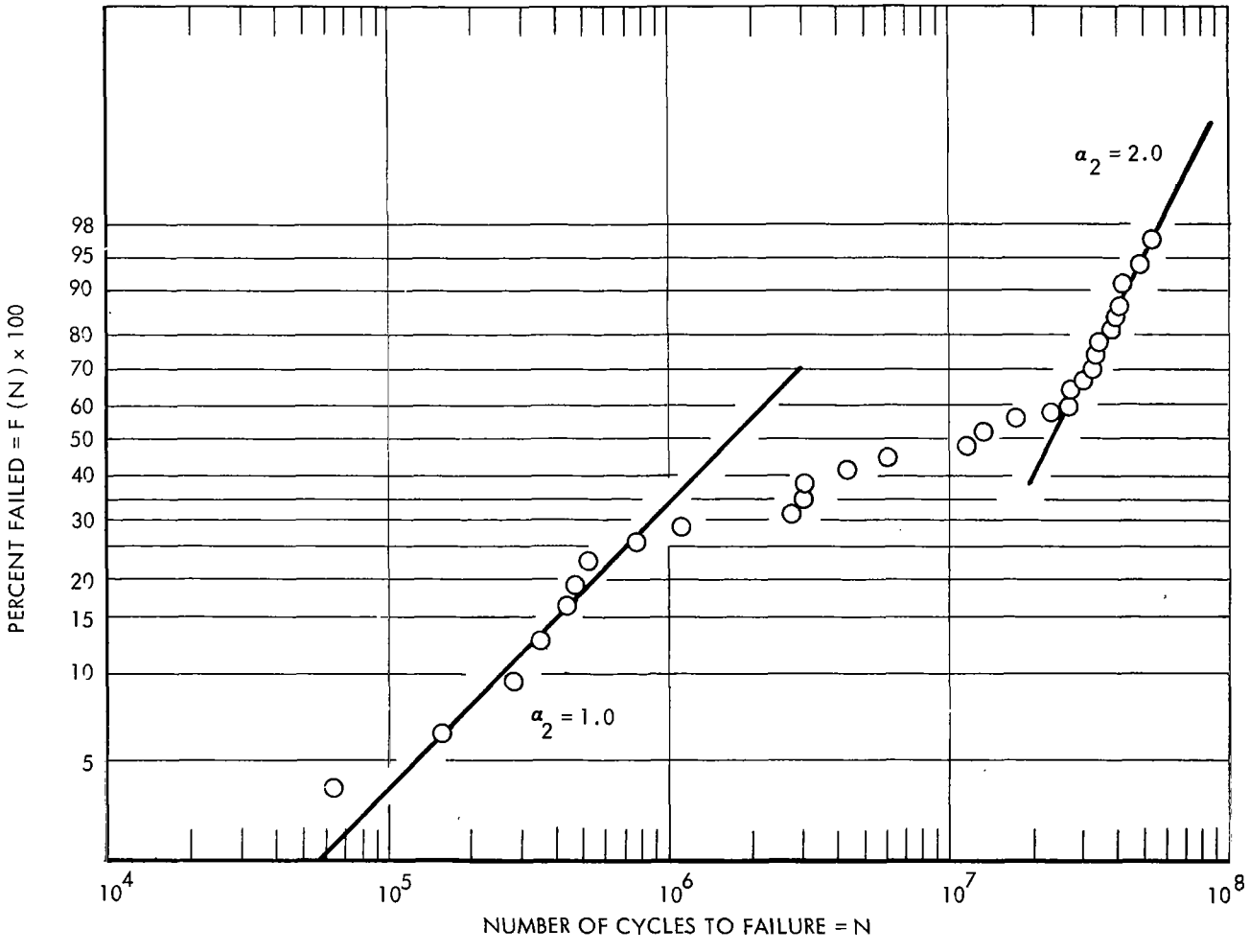

FIGURE 23 - WEIBULL DISTRIBUTION FOR HIGH FREQUENCY FATIQUE FOR ANNEALED TITANIUM 6AL-4V

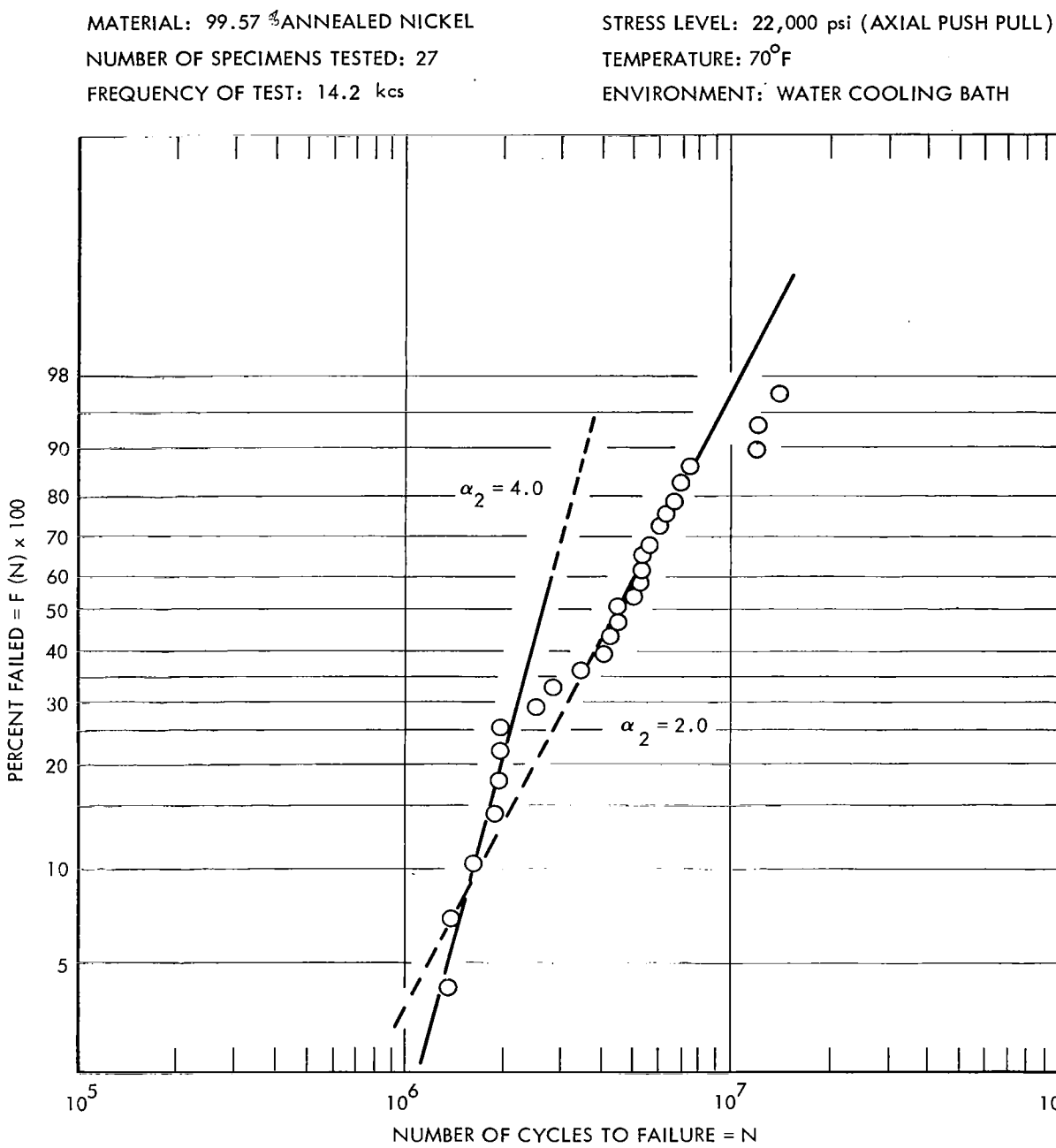

FIGURE 24 - WEIBULL DISTRIBUTION FOR HIGH FREQUENCY FATIGUE OF ANNEALED 99.57 % NICKEL

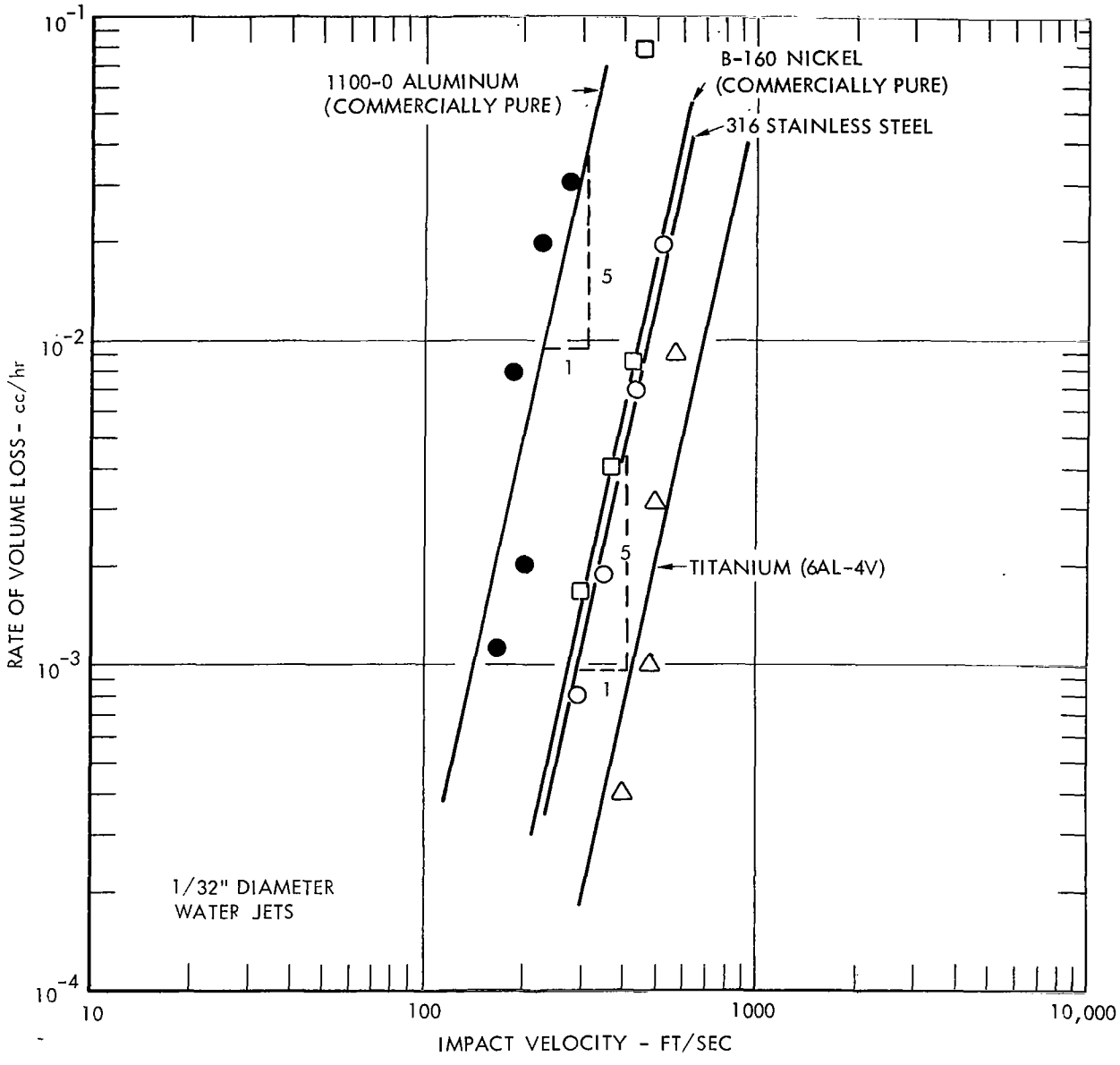

FIGURE 25 - RELATIONSHIP BETWEEN PEAK RATE OF VOLUME LOSS AND THE IMPACT VELOCITY

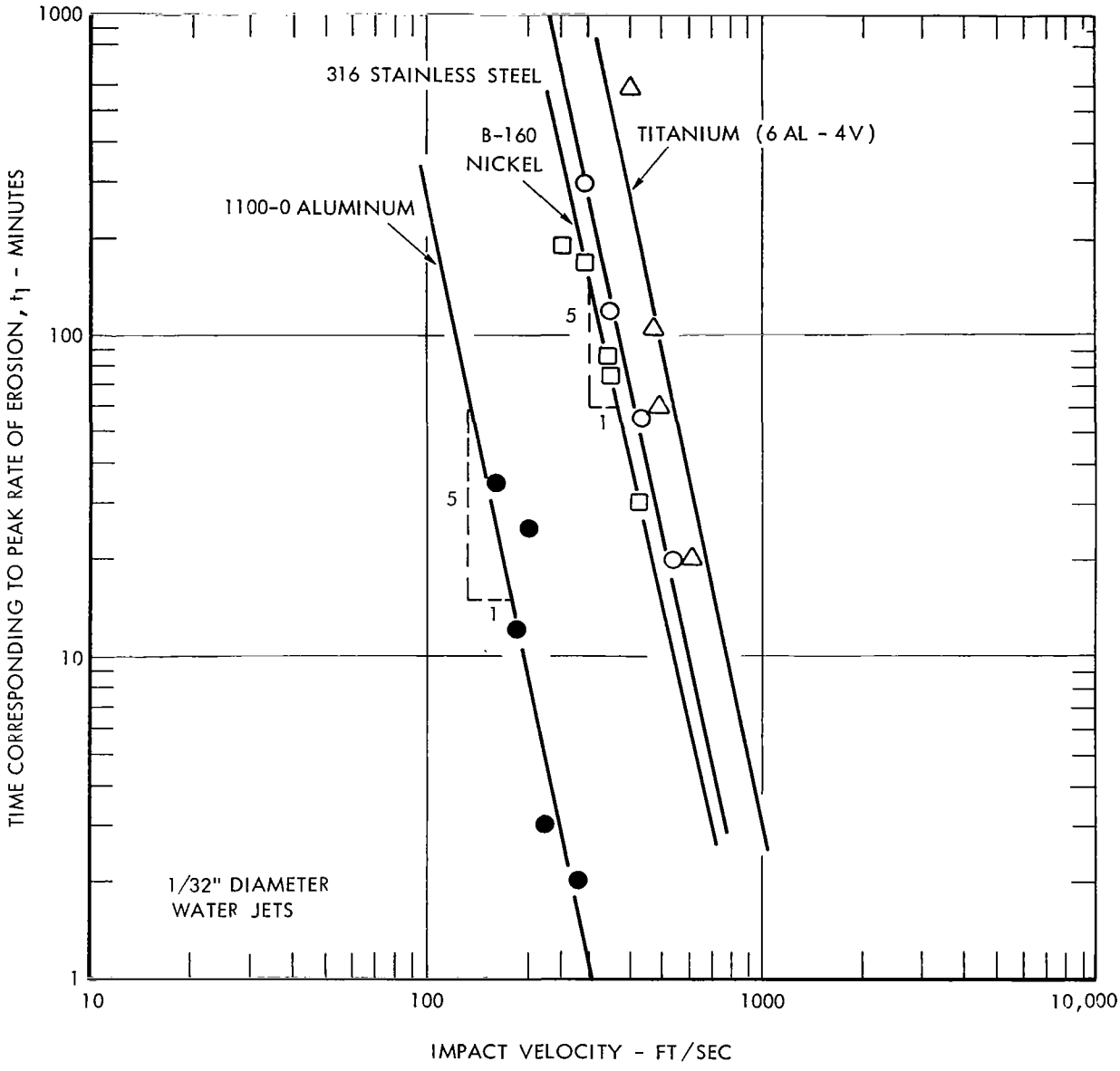

FIGURE 26 - RELATIONSHIP BETWEEN THE TIME AT WHICH PEAK RATE IS OBSERVED AND THE IMPACT VELOCITY

MATERIAL:	99.57% NICKEL (ANNEALED)	FREQUENCY:	13.5 kcs
DENSITY:	8.9 g/cc	SPECIMEN DIAMETER:	0.375 inch
DOUBLE AMPLITUDE:	3×10^{-3} inch	TEST LIQUID:	DISTILLED WATER AT 68° F

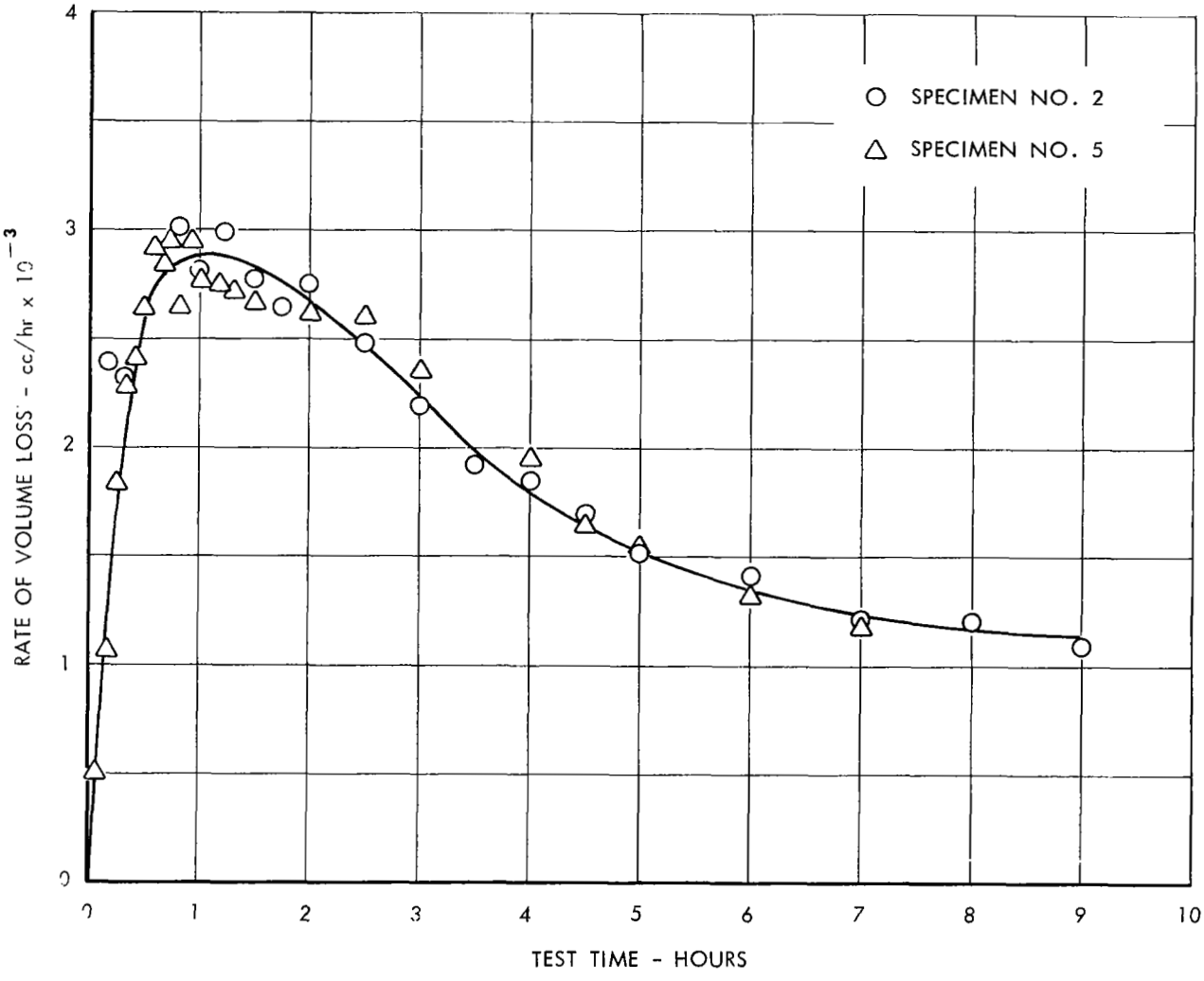

FIGURE 27 - RESULTS OF CAVITATION EROSION TESTS ON COMMERCIALLY PURE ANNEALED NICKEL

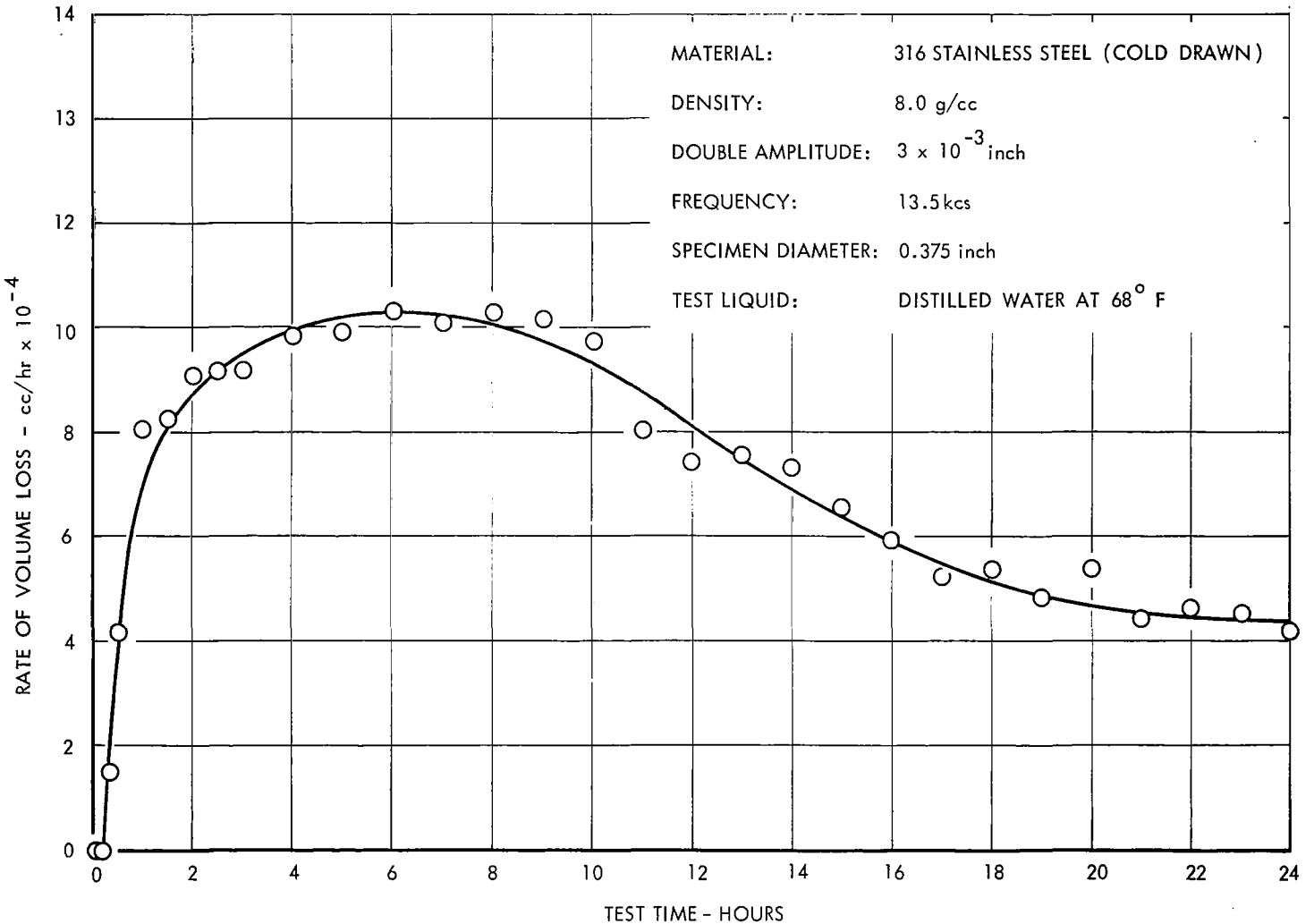

FIGURE 28 - RESULTS OF CAVITATION EROSION TESTS ON 316 STAINLESS STEEL

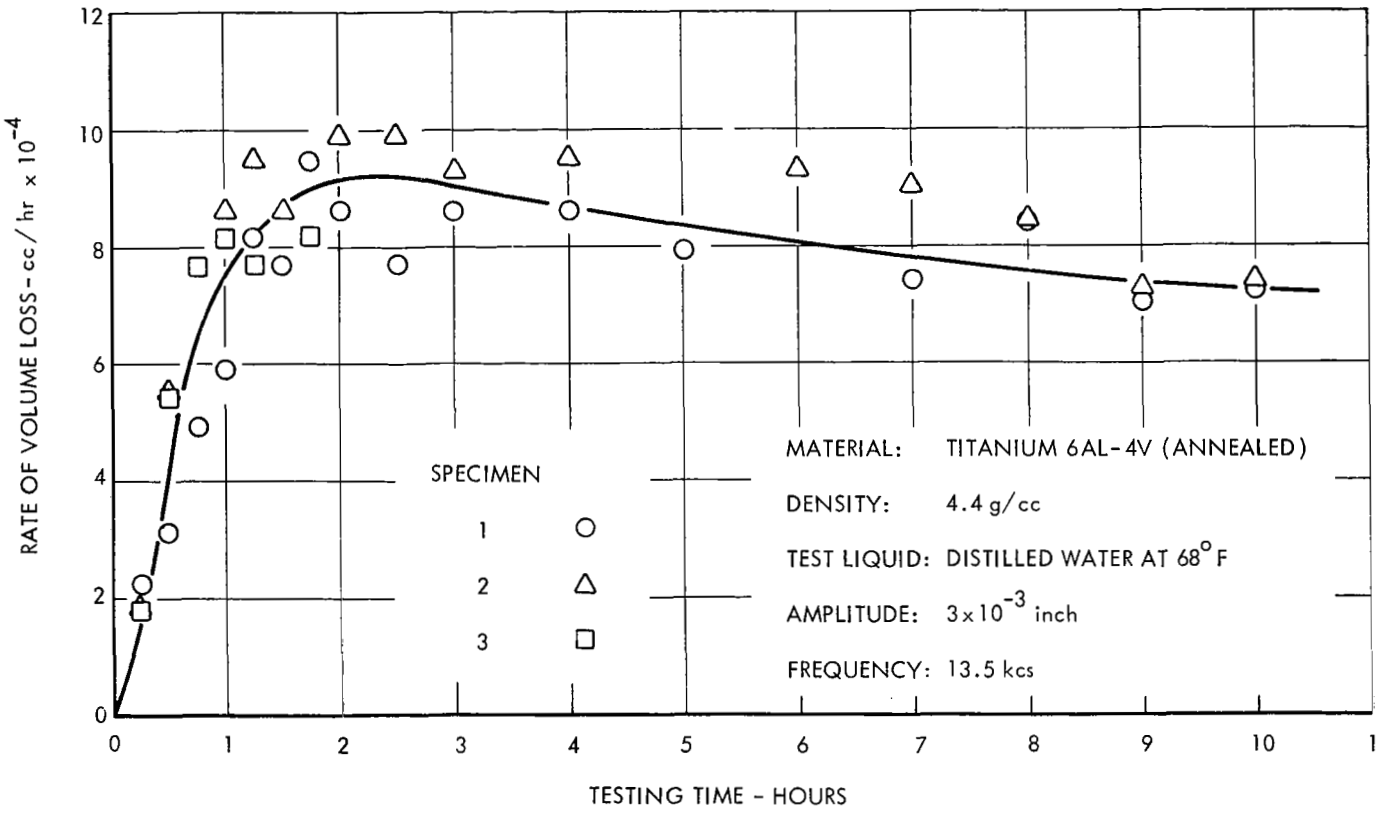

FIGURE 29 - RESULTS OF CAVITATION EROSION TESTS ON TITANIUM 6 AL - 4V

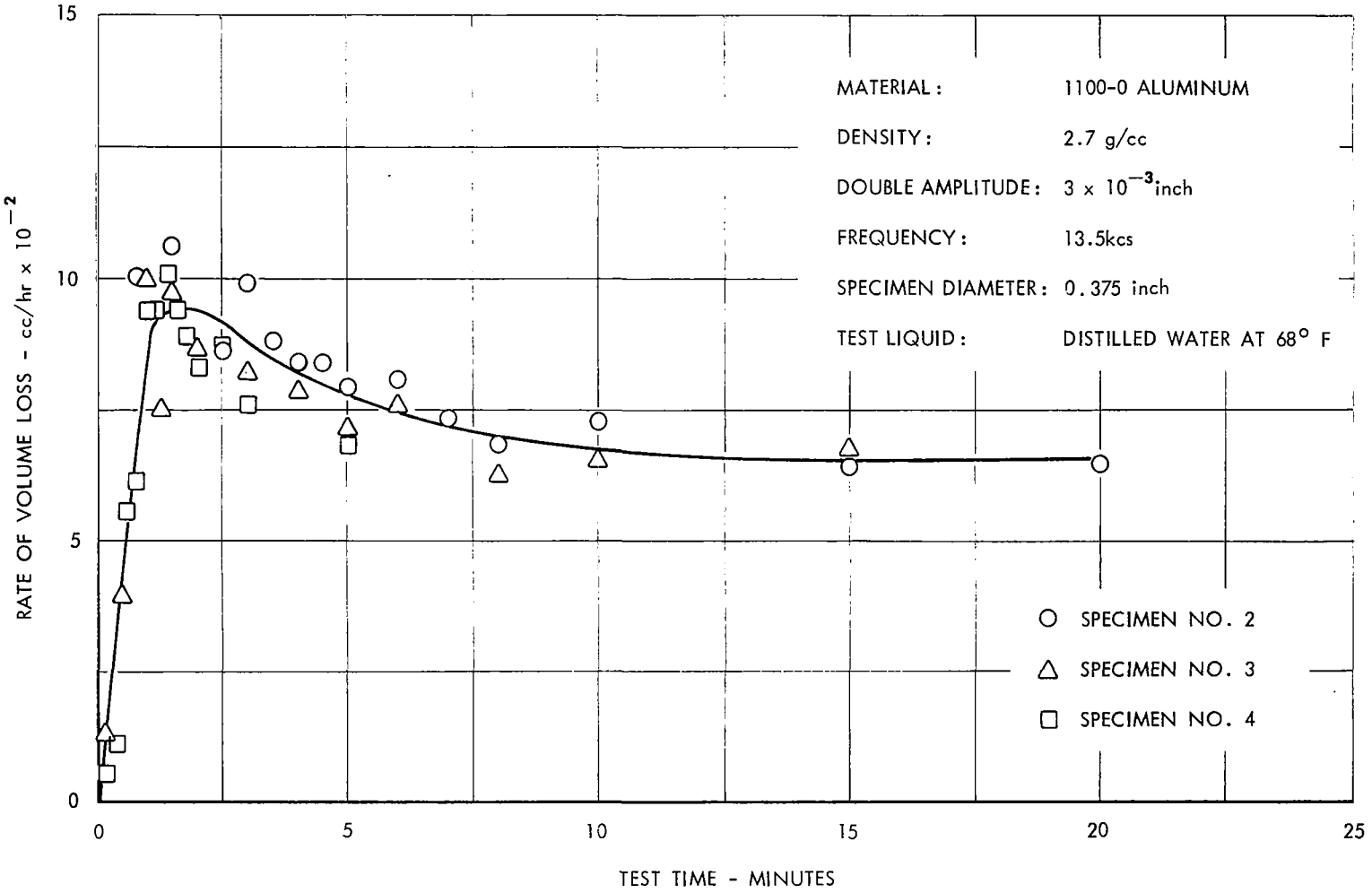

FIGURE 30 - RESULTS OF CAVITATION EROSION TESTS ON 1100 - 0 ALUMINUM

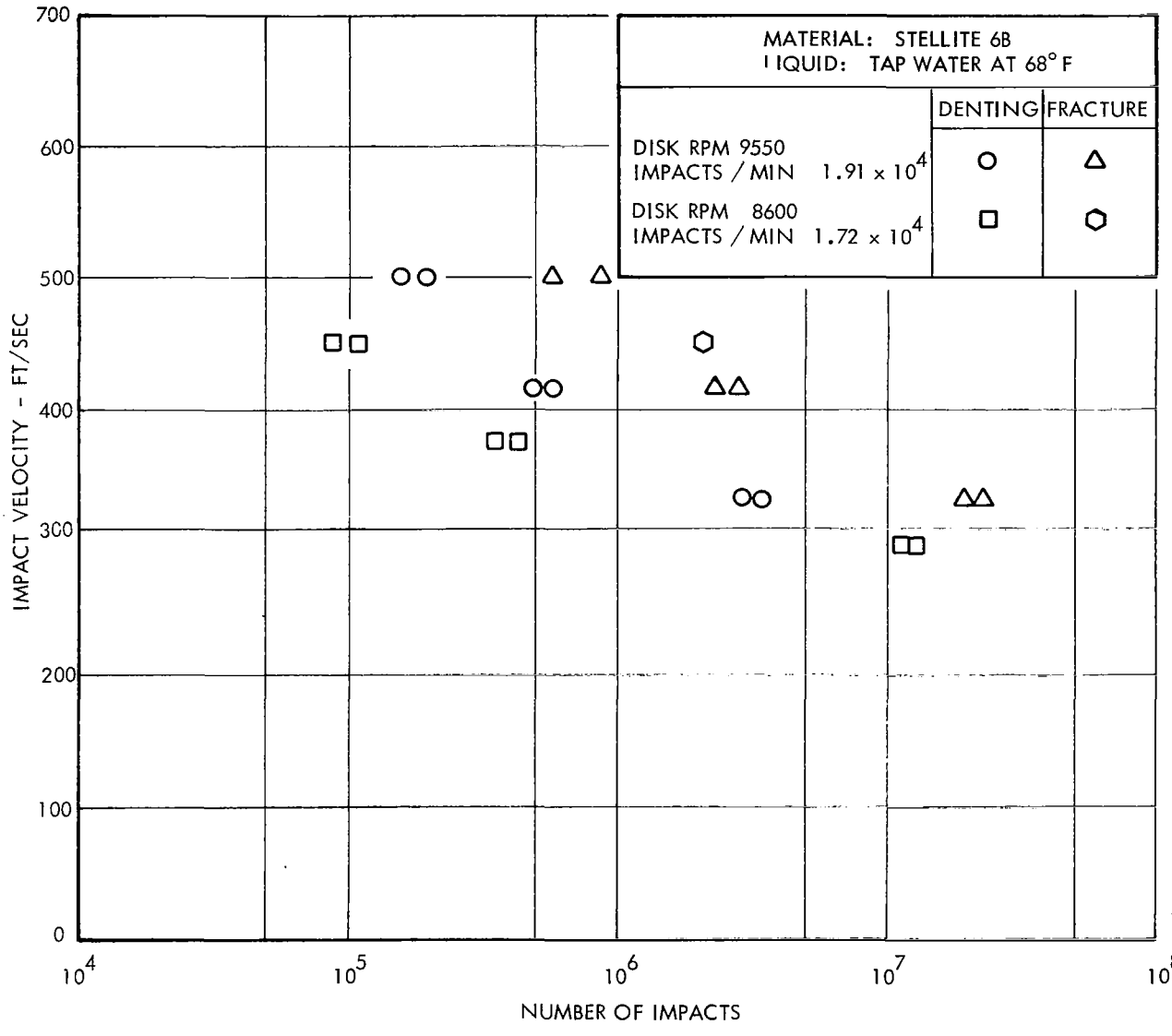

FIGURE 31 - RELATION BETWEEN IMPACT VELOCITY AND THE NUMBER OF IMPACTS AT WHICH EROSION IS OBSERVED ON STELLITE - 6B

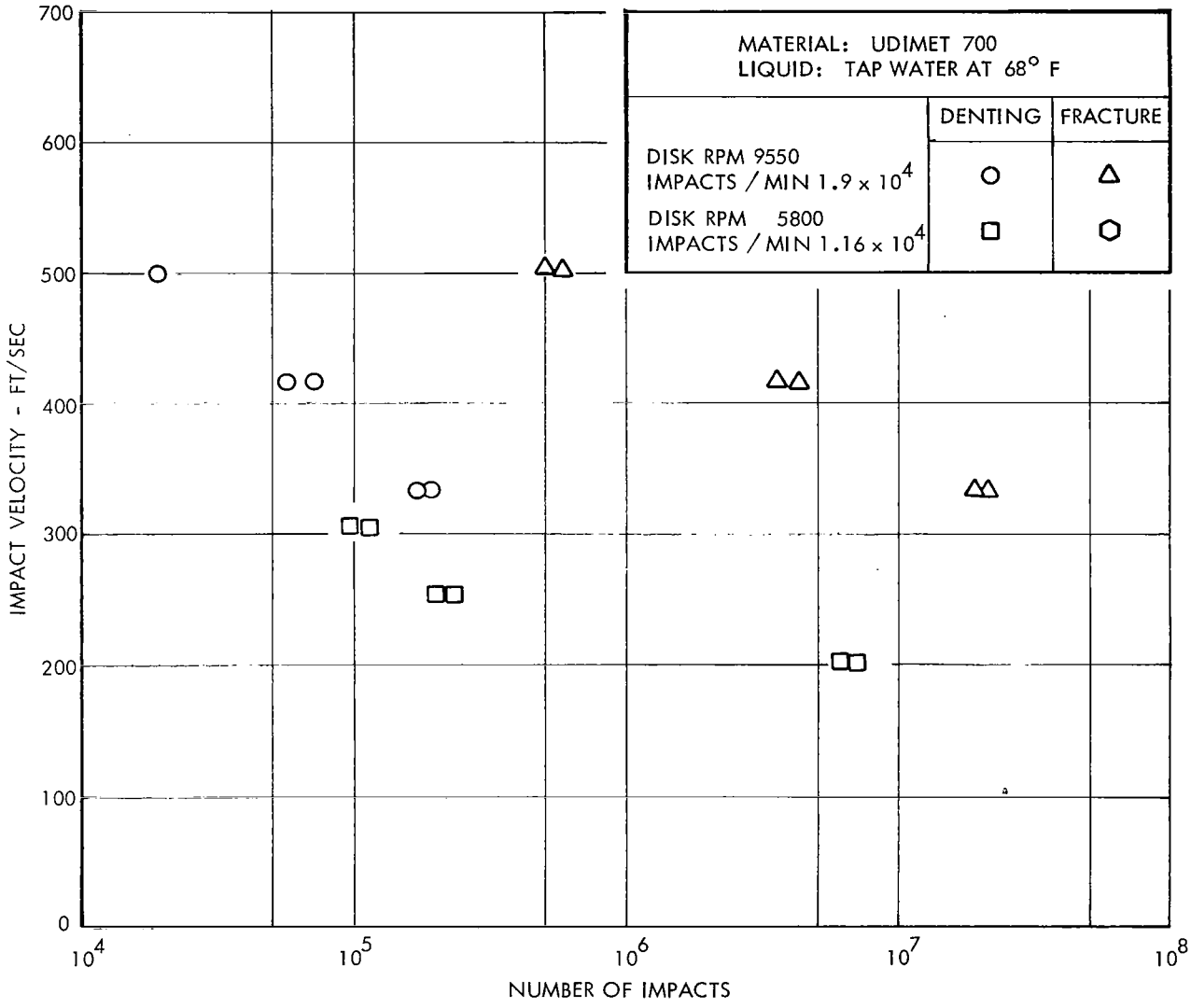

FIGURE 32 - RELATION BETWEEN IMPACT VELOCITY AND THE NUMBER OF IMPACTS AT WHICH EROSION IS OBSERVED ON UDIMET 700

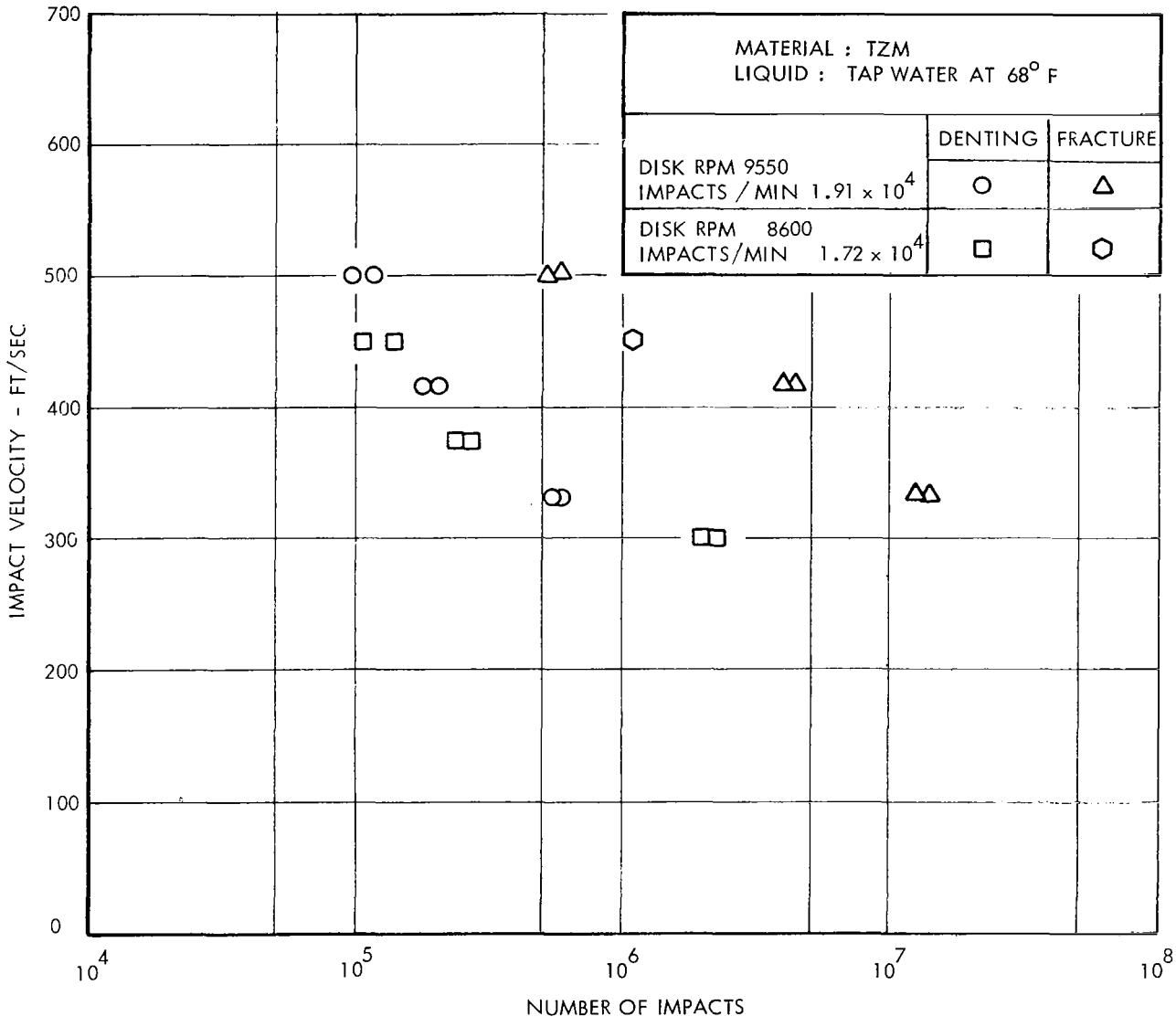

FIGURE 33 - RELATION BETWEEN IMPACT VELOCITY AND THE NUMBER OF IMPACTS AT WHICH EROSION IS OBSERVED ON TZM

NASA-Langley, 1970 —— 32 CR-1638